



## UvA-DARE (Digital Academic Repository)

### **A companion to the preclinical common data elements and case report forms for in vivo rodent Neuroimaging**

*A report of the TASK3-WG3 Neuroimaging Working Group of the ILAE/AES Joint Translational Task Force*

van Vliet, E.A.; Immonen, R.; Prager, O.; Friedman, A.; Bankstahl, J.P.; Wright, D.K.; O'Brien, T.J.; Potschka, H.; Gröhn, O.; Harris, N.G.

**DOI**

[10.1002/epi4.12643](https://doi.org/10.1002/epi4.12643)

**Publication date**

2025

**Document Version**

Final published version

**Published in**

Epilepsia Open

**License**

CC BY-NC-ND

[Link to publication](#)

**Citation for published version (APA):**

van Vliet, E. A., Immonen, R., Prager, O., Friedman, A., Bankstahl, J. P., Wright, D. K., O'Brien, T. J., Potschka, H., Gröhn, O., & Harris, N. G. (2025). A companion to the preclinical common data elements and case report forms for in vivo rodent Neuroimaging: A report of the TASK3-WG3 Neuroimaging Working Group of the ILAE/AES Joint Translational Task Force. *Epilepsia Open*, 10(S1), S136-S182. <https://doi.org/10.1002/epi4.12643>

**General rights**



It is not permitted to download or to forward/distribute the text or part of it without the consent of the author(s) and/or copyright holder(s), other than for strictly personal, individual use, unless the work is under an open content license (like Creative Commons).

**Disclaimer/Complaints regulations**

If you believe that digital publication of certain material infringes any of your rights or (privacy) interests, please let the Library know, stating your reasons. In case of a legitimate complaint, the Library will make the material inaccessible and/or remove it from the website. Please Ask the Library: <https://uba.uva.nl/en/contact>, or a letter to: Library of the University of Amsterdam, Secretariat, P.O. Box 19185, 1000 GD Amsterdam, The Netherlands. You will be contacted as soon as possible. University of Amsterdam (<https://dare.uva.nl>)

## SPECIAL REPORT

# A companion to the preclinical common data elements and case report forms for in vivo rodent neuroimaging: A report of the TASK3-WG3 Neuroimaging Working Group of the ILAE/AES Joint Translational Task Force

Erwin A. van Vliet<sup>1,2</sup>  | Riikka Immonen<sup>3</sup> | Ofer Prager<sup>4</sup>  | Alon Friedman<sup>4,5</sup>  |  
 Jens P. Bankstahl<sup>6</sup>  | David K. Wright<sup>7</sup>  | Terence J. O'Brien<sup>8</sup>  |  
 Heidrun Potschka<sup>9</sup>  | Olli Gröhn<sup>3</sup>  | Neil G. Harris<sup>10,11</sup> 

<sup>1</sup>Center for Neuroscience, Swammerdam Institute for Life Sciences, University of Amsterdam, Amsterdam, The Netherlands

<sup>2</sup>Amsterdam UMC Location University of Amsterdam, Department of (Neuro)Pathology, Amsterdam Neuroscience, Amsterdam, The Netherlands

<sup>3</sup>A.I. Virtanen Institute, University of Eastern Finland, Kuopio, Finland

<sup>4</sup>Departments of Physiology and Cell Biology, Cognitive and Brain Sciences, Zlotowski Center for Neuroscience, Ben-Gurion University of the Negev, Beer-Sheva, Israel

<sup>5</sup>Department of Medical Neuroscience and Brain Repair Center, Dalhousie University, Halifax, Nova Scotia, Canada

<sup>6</sup>Department of Nuclear Medicine, Hannover Medical School, Hannover, Germany

<sup>7</sup>Department of Neuroscience, Central Clinical School, Monash University, Melbourne, Victoria, Australia

<sup>8</sup>The Royal Melbourne Hospital, The University of Melbourne, The Alfred Hospital, Monash University, Melbourne, Victoria, Australia

<sup>9</sup>Institute of Pharmacology, Toxicology, and Pharmacy, Ludwig-Maximilians-University, Munich, Germany

<sup>10</sup>Department of Neurosurgery UCLA, UCLA Brain Injury Research Center, Los Angeles, California, USA

<sup>11</sup>Intellectual and Developmental Disabilities Research Center, UCLA, Los Angeles, California, USA

## Correspondence

Erwin A. van Vliet, Center for Neuroscience, Swammerdam Institute for Life Sciences, University of Amsterdam, PO box 94246, 1090 GE, Amsterdam, The Netherlands.

Email: [e.a.vanvliet@uva.nl](mailto:e.a.vanvliet@uva.nl)

Neil G. Harris, UCLA Brain Injury Research Center, Department of Neurosurgery UCLA, 300 Stein Plaza, Los Angeles, CA 90095, USA.

Email: [ngharris@ucla.edu](mailto:ngharris@ucla.edu)

## Abstract

The International League Against Epilepsy/American Epilepsy Society (ILAE/AES) Joint Translational Task Force established the TASK3 working groups to create common data elements (CDEs) for various aspects of preclinical epilepsy research studies, which could help improve the standardization of experimental designs. In this article, we discuss CDEs for neuroimaging data that are collected in rodent models of epilepsy, with a focus on adult rats and mice. We provide detailed CDE tables and case report forms (CRFs), and with this companion manuscript, we discuss the methodologies for several imaging modalities and the parameters that can be collected.

## KEYWORDS

epilepsy, rat, mouse, magnetic resonance imaging, magnetic resonance spectroscopy, positron emission tomography, single photon emission computed tomography

This is an open access article under the terms of the [Creative Commons Attribution-NonCommercial-NoDerivs](https://creativecommons.org/licenses/by-nc-nd/4.0/) License, which permits use and distribution in any medium, provided the original work is properly cited, the use is non-commercial and no modifications or adaptations are made.

© 2022 The Authors. *Epilepsia Open* published by Wiley Periodicals LLC on behalf of International League Against Epilepsy.

## 1 | INTRODUCTION

For some time now it has been recognized that there are many benefits to the sharing and reuse of data across laboratories. Not least is the fact that this may lead to new discoveries that would not have been possible with data from a single laboratory alone. This potential has been brought about by new data analytics headed by tools such as machine and deep learning, spurred on by enhancement in computer design and storage capabilities. In order to fully capitalize on this potential, the collected “big data” must be somewhat uniformly acquired and archived in a manner that makes it accessible for further processing. Data acquisition according to a predefined framework is the idea behind Common Data Elements (CDEs) that have garnered both clinical and now preclinical support by NIH (<https://commondataelements.ninds.nih.gov/>). Construction and eventual mainstream use of CDE are advantageous because it embodies the FAIR principles of Findability, Accessibility, Interoperability, and Reusability<sup>1</sup> that facilitate data and information sharing in a robust and ethical way.

Preclinical neuroimaging data are commonly acquired in epilepsy research since whole brain coverage can usually be obtained and imaging is minimally or noninvasive and therefore allows multiple data snapshots to be acquired to follow the disease process. There are many imaging techniques that can be applied to study specific pathological alterations in the epileptogenic brain, on a structural or functional level (Figure 1). To date, however, there have been no formal attempts to standardize the acquisition process across laboratories involved in epilepsy research. Given, for example, the recent formation of the Epilepsy Bioinformatics Study for Antiepileptogenic Therapy (EpiBioS4Rx), a large international, multicenter Center without Walls (CWOW; <https://epibios.loni.usc.edu/>) that requires preclinical data acquisition from multiple sites across the world, there is a pressing need to formalize common methods to potentiate the current and future use of these type of data. In a recent paper, a proposal was made to harmonize a pipeline for preclinical multicenter MRI biomarker discovery in a rat model for post-traumatic epileptogenesis.<sup>2</sup> We further elaborated on that and have organized the CDEs into a set of case report forms (CRFs) that will provide a more streamlined approach to reconciling differences in acquisition protocols across sites when data harmonization is required for a shared project, with a main focus on preclinical rodent epilepsy models but also making the bridge to the clinic.

### Key Points

1. This joint ILAE/AES initiative introduces common data elements (CDEs) related to the measurement of various neuroimaging parameters in adult rodents.
2. Case report forms (CRFs) and a companion report discussing their use are provided for the various neuroimaging modalities.
3. Future use of these forms may help to standardize animal experiments and to improve and facilitate meta-analysis studies.

## 2 | METHODS

*The Neuroimaging group* consists of 10 (pre)clinical epilepsy imaging researchers, selected on their relevant expertise who developed CDEs and CRFs for 11 neuroimaging modules (see following paragraphs).

The CDEs/CRFs are organized around the following modules: (1) Technical Information, (2) Physiology, (3) Contrast-Enhanced Magnetic Resonance Imaging for blood–brain barrier permeability, (4) Angiography, (5) Arterial Spin Labeling, (6) Diffusion-Weighted Magnetic Resonance Imaging, (7) Volumetry, (8) Manganese Contrast-Enhanced Magnetic Resonance Imaging, (9) Functional Magnetic Resonance Imaging, (10) <sup>1</sup>H Magnetic Resonance Spectroscopy, (11) Positron Emission Tomography and Single Photon Emission Computed Tomography. We recommend to complete the CRFs for modules 1 (Technical information) and 2 (Physiology) independent of the imaging method used (high priority CDEs/CRFs) and choose from modules 3–11 the one(s) that fits the imaging method used. For longitudinal studies, the modules 2–11 can be used repetitively. For an overview of the CRFs and their priority, see Table 1.

The forms are constructed in analogy to previous preclinical CDEs by the TASK3 group of the ILAE/AES Joint Translational Task Force.<sup>3–8</sup> CDEs generated by the EPITARGET consortium (Targets and Biomarkers for Antiepileptogenesis)<sup>9</sup> served as useful templates for our working group. The proposed recommendations originate mostly from previously published methods in rodent epilepsy model research. Within the Neuroimaging Working Group, the 11 modules were divided among the members, taking into account their expertise. Each subgroup prepared a draft for the CDE/CRF form and the accompanying part of the manuscript, presented this to the whole group during one of

## Neuroimaging in the epileptogenic brain

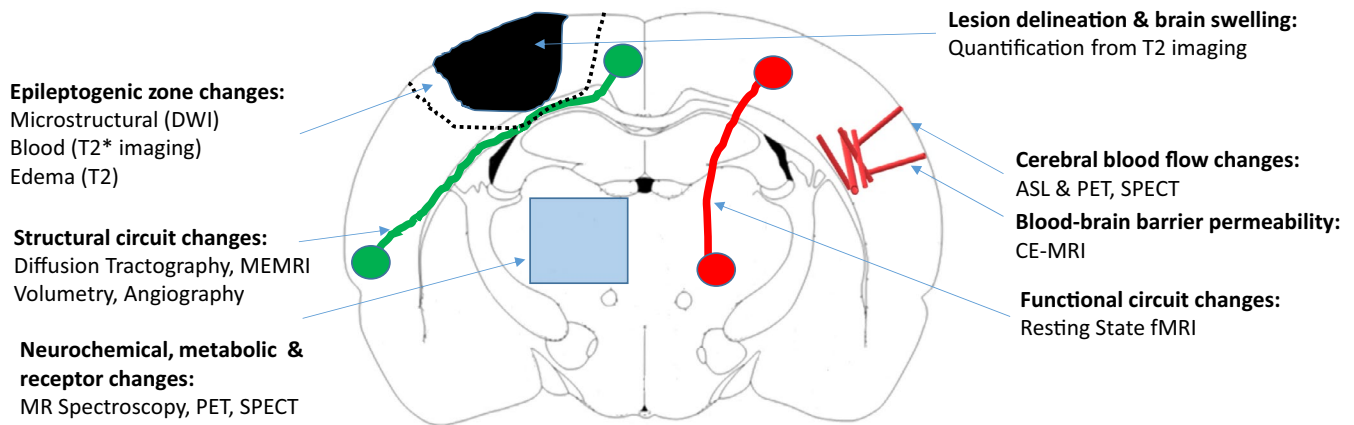


**FIGURE 1** Overview of neuroimaging techniques to detect changes in the epileptic brain. ASL, arterial spin labeling; CE-MRI, contrast-enhanced magnetic resonance imaging; DWI, diffusion-weighted magnetic resonance imaging; fMRI, functional magnetic resonance imaging; MEMRI, manganese-enhanced magnetic resonance imaging; MRS, magnetic resonance spectroscopy; PET, positron emission tomography; SPECT, single photon emission computed tomography.

| CRF number | CRF name  | Priority      |
|------------|---|---------------|
| 1          | Technical information   | High          |
| 2          | Physiology  | High          |
| 3          | Contrast-enhanced magnetic resonance imaging for BBB permeability           | If applicable |
| 4          | Angiography   | If applicable |
| 5          | Arterial spin labeling  | If applicable |
| 6          | Diffusion-weighted magnetic resonance imaging                               | If applicable |
| 7          | Volumetry   | If applicable |
| 8          | Manganese contrast-enhanced magnetic resonance imaging                      | If applicable |
| 9          | Functional magnetic resonance imaging                                       | If applicable |
| 10         | <sup>1</sup> H magnetic resonance spectroscopy                              | If applicable |
| 11         | Positron emission tomography and single photon emission computed tomography | If applicable |

**TABLE 1** Overview of the case report forms (CRFs) and their priority

the 10 Working Group meetings, and the draft was changed until a consensus was reached and all members agreed with the content. The final version includes feedback from members of the TASK3 group and the Task Force.

### 3 | RESULTS

For each neuroimaging module (1-11) we provide a rationale and an overview of the elements that are included in the corresponding CRFs. The CDE and CRF modules linked to this paper are also available as electronic files.

#### 3.1 | Technical information

CRF File name: 01 CRF module - Technical information.docx

CDE File name: 01 CRF module - Technical information.xlsx ([Supporting information](#))

##### 3.1.1 | Rationale

Preclinical neuroimaging can be performed with a large variety of equipment. We aimed to summarize in this CRF

(see also [Figure 2](#)) the technical information of commonly used equipment for neuroimaging in rodents.

### 3.1.2 | Measurements

The most commonly used modalities for small animal in vivo imaging applications are based on computed tomography (CT), magnetic resonance imaging (MRI), angiography, positron emission tomography (PET), and single photon emission computed tomography (SPECT), which can be used to identify specific disease processes. Furthermore, optical imaging and ultrasound can be used, but these are not covered here. Since each modality has advantages and limitations, multimodal imaging is becoming more popular and by combining several imaging modalities, complementary information about the pathophysiological processes underlying epileptogenesis can be obtained.

### 3.1.3 | Equipment

Today, the main magnetic field strength for neuroimaging in mice and rats is typically above 7 T. Lower field strengths can be used, but this leads to loss of spatial information, and therefore, field strengths less than 4.7 T are not recommended. A modern MRI system has actively shielded gradients with strengths higher than ~500 mT and good eddy-current (the electrical current induced by a changing magnetic field according to Faraday's law of induction) behavior. The combination of a volume/transmit coil and a local receiver coil, with a good filling factor (defined as the ratio of the magnetic field energy stored inside the sample volume versus the total magnetic energy stored by the radiofrequency coil) size-matched to the target tissue, and 2-8 receiver channels are optimal for most applications. Cryogenic radiofrequency coils can provide significant signal-to-noise improvement. With this kind of hardware the MRI system should achieve equivalent

#### Neuroimaging Studies

Case Report Form: 01 CRF – Technical information.docx

CRF module: Technical information

Date and time that this CRF was filled out:

Name of person filling out CRF:

Project name/Identifier:

Animal ID:

| CDE Name                     | Data Collected  |
|------------------------------|---|
| <b>Imaging modality</b>      |   |
| Imaging modality used        | <input type="checkbox"/> Computed Tomography<br><input type="checkbox"/> Magnetic Resonance Imaging<br><input type="checkbox"/> Positron Emission Tomography<br><input type="checkbox"/> Single Photon Emission Computed Tomography<br><input type="checkbox"/> Unknown<br><input type="checkbox"/> Other |
| If other, please specify     |   |
| Main magnetic field strength | <input type="checkbox"/> 4.7 T<br><input type="checkbox"/> 7.0 T<br><input type="checkbox"/> 9.4 T<br><input type="checkbox"/> 11.7 T<br><input type="checkbox"/> Unknown<br><input type="checkbox"/> Other   |
| If other, please specify     |   |
| Imaging scanner manufacturer | <input type="checkbox"/> Agilent<br><input type="checkbox"/> Bruker<br><input type="checkbox"/> GE Healthcare<br><input type="checkbox"/> Hitachi<br><input type="checkbox"/> Mrsolution  |

FIGURE 2 Technical information case report form (see main text for details)

|   |  |
|---|--|
|   | <input type="checkbox"/> Philips<br><input type="checkbox"/> Siemens<br><input type="checkbox"/> Unknown<br><input type="checkbox"/> Other   |
| If other, please specify                |  |
| Imaging scanner model name              |  |
| Imaging scanner software version number |  |
| <b>Gradient coil</b>                    |  |
| Gradient coil manufacturer              |  |
| Gradient coil type                      |  |
| Strength in mT/m                        |  |
| Maximum linear slew rate in T/m/s       |  |
| <b>Shim coil</b>                        |  |
| Shim coil manufacturer                  |  |
| Shim type                               | <input type="checkbox"/> Passive<br><input type="checkbox"/> Active superconductive<br><input type="checkbox"/> Active resistive<br><input type="checkbox"/> Unknown<br><input type="checkbox"/> Other |
| If other, please specify                |  |
| Shim method                             | <input type="checkbox"/> Auto <input type="checkbox"/> Dynamic <input type="checkbox"/> Local <input type="checkbox"/> Unknown<br><input type="checkbox"/> Other                                       |
| If other, please specify                |  |
| <b>Radiofrequency coil</b>              |  |
| Volume transmitter                      | <input type="checkbox"/> Actively decoupled volume transmitter   |

FIGURE 2 (Continued)

anatomical resolution as in humans and reach a voxel size of less than  $200 \mu\text{m}^2$  (in-plane) and  $200 \mu\text{m}$  to  $1 \text{ mm}$  slice thickness<sup>10</sup> and be capable of obtaining imaging data with fast pulse sequences for functional MRI (fMRI) and diffusion tensor imaging (DTI) applications. Of course, older or less capable hardware can still be employed to conduct studies and contribute important information. However, this normally incurs a time penalty due to the longer imaging time to achieve a usable image signal-to-noise, or a spatial penalty, for example, due to longer gradient ramp times leading to fewer slice acquisitions within a standard repetition time. An important part of the instrumentation is the animal holder that should have ear bars, bite bar, heating element, and mounting for basic physiological monitoring probes for accurate, reproducible, and fast positioning of animals for large-scale longitudinal studies.

The recommended *procedure* (including the imaging sequence, which is specific for the disease process studied)

as well as the *analysis and interpretation* are summarized for each imaging modality in the following sections.

## 3.2 | Physiology

CRF File name: 02 CRF module - Physiology.docx

CDE File name: 02 CDE chart - Physiology.xlsx  
[\(Supporting information\)](#)

### 3.2.1 | Rationale

Animals are typically anesthetized for neuroimaging and it is important to monitor and maintain their physiological condition within an appropriate physiological range. It is important to consider the choice of anesthesia carefully, as it has a profound impact on many imaging

|  |   |
|--|---|
|  | <input type="checkbox"/> Multichannel actively decoupled volume transmitter<br><input type="checkbox"/> Unknown<br><input type="checkbox"/> Other |
| If actively decoupled volume transmitter; please specify type                            | <input type="checkbox"/> Linear<br><input type="checkbox"/> Quadrature<br><input type="checkbox"/> Unknown  |
| If multichannel actively decoupled volume transmitter, please specify number of channels |   |
| If other type of volume transmitter, please specify                                      |   |
| Receiver   | <input type="checkbox"/> Local receiver<br><input type="checkbox"/> Unknown<br><input type="checkbox"/> Other                                     |
| If local receiver, please specify type   | <input type="checkbox"/> Linear<br><input type="checkbox"/> Quadrature<br><input type="checkbox"/> Unknown  |
| If other, please specify   |   |
| Coil size in cm  |   |
| Cryoprobe  | <input type="checkbox"/> No <input type="checkbox"/> Yes<br><input type="checkbox"/> Unknown  |
| If cryoprobe used, please specify type   |   |

**Instructions:** Please check boxes where applicable. If none of the predetermined options is appropriate use the default space to specify your answer. This form is to be filled in for one individual animal.

FIGURE 2 (Continued)

parameters.<sup>11,12</sup> More imaging method-specific information on anesthesia effects is provided with the CDEs/CRFs where applicable.

The level of monitoring depends on the application; however, it should be noted that the measurement of typical brain MRI relaxation times and water diffusivity depends on both temperature and cerebral blood flow, the latter of which is highly dependent upon blood pCO<sub>2</sub>, which has profound effects on arterial spin labeling and fMRI signal intensity. Maintaining physiological status within a normal range during anesthesia will not only improve reliability and reproducibility of the imaging data but also facilitate recovery from anesthesia and an overall beneficial effect on the animal outcome. In the accompanying CRF (see also Figure 3) the main physiological parameters are described.

### 3.2.2 | Measurements

As a minimum requirement, respiration rate and body temperature should be monitored for every experiment, while oxygenation and CO<sub>2</sub> level are important for fMRI and

arterial spin labeling experiments. Heart rate and blood pressure measurements can provide additional information about the depth of anesthesia. Respiration and cardiac monitoring are also required if the acquisition is to be triggered, e.g., for high resolution, echo-planar-based acquisitions.

### 3.2.3 | Equipment

Temperature control is typically performed with a rectal probe. The animal's body temperature drops rapidly during anesthesia and a heating system consisting of either hot water circulation or warm air is used to maintain normal body temperature. Optimally, heating is homeostatically controlled by additional circuitry within the controller. Respiration rate can be measured using a pressure sensor positioned beneath, or over, the animal's diaphragm.

### 3.2.4 | Procedure

Anesthesia affects brain activity and neurovascular coupling and this can have profound effects on fMRI

## Neuroimaging Studies

Case Report Form: 02 CRF – Physiology.docx

CRF module: Physiology

Date and time that this CRF was filled out:

Name of person filling out CRF:

Project name/Identifier:

Animal ID:

| CDE Name                                     | Data Collected  |
|--|---|
| <b>Anesthesia during preparatory surgery</b> |   |
| Anesthesia during imaging                    | <input type="checkbox"/> Yes <input type="checkbox"/> No <input type="checkbox"/> Unknown   |
| If anesthesia was administered, specify type | <input type="checkbox"/> Isoflurane <input type="checkbox"/> Sevoflurane <input type="checkbox"/> Ketamine/Xylazine<br><input type="checkbox"/> Pentobarbitone <input type="checkbox"/> Medetomidine<br><input type="checkbox"/> Alphachloralose <input type="checkbox"/> Urethane <input type="checkbox"/> Unknown<br><input type="checkbox"/> Other |
| If other, please specify                     |   |
| Route of administration                      | <input type="checkbox"/> Intramuscular <input type="checkbox"/> Intraperitoneal <input type="checkbox"/> Intravenous<br><input type="checkbox"/> Inhalational <input type="checkbox"/> Unknown <input type="checkbox"/> Other   |
| If other, please specify                     |   |
| Isoflurane concentration induction %         |   |
| Isoflurane concentration maintenance %       |   |
| Sevoflurane concentration induction %        |   |
| Sevoflurane concentration maintenance %      |   |
| Ketamine dose in mg/kg                       |   |
| Xylazine dose in mg/kg                       |   |
| Pentobarbitone dose in mg/kg                 |   |
| Medetomidine dose in mg/kg                   |   |
| Alphachloralose dose in mg/kg                |   |
| Urethane dose in mg/kg                       |   |

FIGURE 3 Physiology case report form (see main text for details)

studies,<sup>13–15</sup> see also Table 2. Unlike structural MRI studies, isoflurane anesthesia should not be used for functional studies as isoflurane causes vasodilatation and hypotension, increases basal blood flow, and in higher doses causes burst suppression activity.<sup>16</sup> Medetomidine sedation has been shown to not suppress epileptiform activity<sup>15</sup> and the combination of 0.5% isoflurane and medetomidine maintains a similar functional connectivity pattern to that obtained in awake animals<sup>17</sup> and therefore both are commonly used for longitudinal studies.<sup>18</sup> Urethane and alpha-chloralose are common choices for fMRI and have been shown to provide robust fMRI responses in evoked activity studies.<sup>19</sup> However, these anesthetics can only be used in terminal experiments and state transitions under urethane anesthesia should be accounted for during the analysis of the data.<sup>20</sup> It should be noted that modulation of functional connectivity by anesthesia is not uniform over the whole brain and, for example, the cortico-thalamic connection is suppressed already

by a subanesthetic dose of isoflurane, which has mostly nonsignificant effects on connectivity.<sup>21</sup>

Postmortem imaging can also be performed. Typically, animals are perfused under anesthesia via the ascending aorta using saline, followed by a fixative (most often formalin or paraformaldehyde) and the brain is scanned *in situ*, or alternatively, the brain is dissected and immersed in fixative or a fluorocarbon-based polymer (e.g., Fomblin or Fluorinert).

### 3.2.5 | Analysis and interpretation

It is recommended to maintain the rodent body temperature at  $37 \pm 0.5^\circ\text{C}$ , the respiratory rate between 50 and 75 breaths per minute (under isoflurane anesthesia), and the total anesthesia time under 2 h<sup>2</sup> to maintain homeostasis, which is crucial for the assessment of functional/metabolic parameters measured. It should be noted that

|   |   |
|---|---|
| Other anesthesia dose in mg/kg  |   |
| Starting time of anesthesia in hours and minutes                        |   |
| Total anesthesia duration in minutes                                    |   |
| Time between cessation of preparatory anesthesia and imaging in minutes |   |
| <b>Anesthesia during imaging</b>  |   |
| Anesthesia during imaging   | <input type="checkbox"/> Yes <input type="checkbox"/> No <input type="checkbox"/> Unknown   |
| If anesthesia was administered, specify type                            | <input type="checkbox"/> Isoflurane <input type="checkbox"/> Sevoflurane <input type="checkbox"/> Ketamine/Xylazine<br><input type="checkbox"/> Pentobarbitone <input type="checkbox"/> Medetomidine<br><input type="checkbox"/> Alphachloralose <input type="checkbox"/> Urethane <input type="checkbox"/> Unknown<br><input type="checkbox"/> Other |
| If other, please specify  |   |
| Route of administration   | <input type="checkbox"/> Intramuscular <input type="checkbox"/> Intraperitoneal <input type="checkbox"/> Intravenous<br><input type="checkbox"/> Inhalational <input type="checkbox"/> Other  |
| If other, please specify  |   |
| Isoflurane concentration induction %                                    |   |
| Isoflurane concentration maintenance %                                  |   |
| Sevoflurane concentration induction %                                   |   |
| Sevoflurane concentration maintenance %                                 |   |
| Ketamine dose in mg/kg  |   |
| Xylazine dose in mg/kg  |   |
| Pentobarbitone dose in mg/kg  |   |
| Medetomidine dose in mg/kg  |   |
| Alphachloralose dose in mg/kg   |   |
| Urethane dose in mg/kg  |   |
| Other anesthesia dose in mg/kg  |   |
| Starting time of anesthesia in hours and minutes                        |   |
| Total anesthesia duration in minutes                                    |   |
| Animal sacrifice  | <input type="checkbox"/> Decapitation <input type="checkbox"/> Perfusion <input type="checkbox"/> Unknown<br><input type="checkbox"/> Not sacrificed  |
| <b>Respiration</b>  |   |
| Ventilation method used   | <input type="checkbox"/> No <input type="checkbox"/> Yes  |

FIGURE 3 (Continued)

respiratory and heart rates vary between different types of anesthesia and may slowly drop.<sup>12</sup> A normal undisturbed respiratory rate is 70-110/min in rodents, but a fall of 50% is acceptable during anesthesia. Although reference values are provided for unanesthetized animals,<sup>22</sup> a systematic analysis of these parameters and reference values for animals under different types of anesthesia is lacking.

### 3.3 | Contrast-enhanced magnetic resonance imaging for blood–brain barrier permeability

CRF File name: 03 CRF module - Contrast-Enhanced Magnetic Resonance Imaging for Blood–Brain Barrier Permeability.docx

CDE File name: 03 CDE chart - Contrast-Enhanced Magnetic Resonance Imaging for Blood–Brain Barrier Permeability.xlsx ([Supporting information](#))

#### 3.3.1 | Rationale

Contrast-enhanced magnetic resonance imaging (CE-MRI) is being used to detect alterations in blood–brain barrier permeability (BBB) by injecting a paramagnetic contrast agent into the vascular system. Typically, the contrast agent does not cross the BBB under normal conditions. However, during pathological conditions associated with BBB dysfunction, it leaks into the brain neuropil and changes the signal read in brain areas with increased BBB permeability (Figure 4). In the accompanying CRF (see also Figure 5) the most important parameters are described.

|   |   |
|---|---|
| Type of ventilation method used                   | <input type="checkbox"/> Mouth mask<br><input type="checkbox"/> Endotracheal tube<br><input type="checkbox"/> Tracheotomy<br><input type="checkbox"/> Unknown<br><input type="checkbox"/> Other                                 |
| If other, please specify                          |   |
| Company name of ventilation device used           |   |
| Model of ventilation device used                  |   |
| Respiration recording method used                 | <input type="checkbox"/> Pulse-oximeter;<br><input type="checkbox"/> Respiration sensor<br><input type="checkbox"/> Unknown   |
| Company name of respiration recording device used |   |
| Model of respiration recording device used        |   |
| <b>Physiological monitoring</b>                   |   |
| Heart rate recording method used                  | <input type="checkbox"/> No <input type="checkbox"/> Yes  |
| Type of heart rate recording method used          | <input type="checkbox"/> External heart rate sensor<br><input type="checkbox"/> Pulse-oximeter<br><input type="checkbox"/> Implanted ECG Telemetry device<br><input type="checkbox"/> Unknown<br><input type="checkbox"/> Other |
| If other, please specify                          |   |
| Company name of heart rate recording device used  |   |
| Model heart of rate recording device used         |   |
| Temperature recording method used                 | <input type="checkbox"/> No <input type="checkbox"/> Yes  |
| Type of temperature recording method used         | <input type="checkbox"/> Feedback-regulated heating pad<br><input type="checkbox"/> Rectal probe  |

FIGURE 3 (Continued)

### 3.3.2 | Measurements

Proton relaxation times are influenced by the presence of paramagnetic ions from the contrast agent, such as gadolinium ( $Gd^{3+}$ ), which shorten the T1 (longitudinal) and T2 (transversal) relaxation times of surrounding water protons to produce a signal-enhancing effect in T1-weighted imaging or signal decrease in T2-weighted imaging. The efficiency of an agent to shorten relaxation times is dependent on the ligand surrounding the  $Gd^{3+}$  ion and the influence of extrinsic factors including temperature, magnetic field strength, and the tissue environment (water, plasma, or blood).<sup>23</sup>

### 3.3.3 | Equipment

- *MR scanner*: Various preclinical MR systems are available. Higher field strengths (e.g., 7 T or higher) are

recommended for measurements in rodents (particularly mice) to provide enough spatial resolution and sensitivity to detect subtle BBB leakage.

- *Contrast agent*: For the detection of BBB leakage, gadolinium-based contrast agents are most commonly used, but contrast agents based on other paramagnetic ions have been developed, including  $Mn^{2+}$  and iron oxide.<sup>23</sup>
- *Infusion system*: The intravenous route is recommended (although intramuscular injection is an option). In order to administer the contrast agent intravenously, a cannula is inserted, most often in the lateral tail vein, and coupled to an infusion system in which an adjustable pump provides a bolus injection or step-down controlled infusion.

### 3.3.4 | Procedure

Measurements are usually performed under inhalation anesthesia (most commonly used is isoflurane). It is

|   |   |
|---|---|
|   | <input type="checkbox"/> Infrared probe<br><input type="checkbox"/> Unknown<br><input type="checkbox"/> Other   |
| If other, please specify  |   |
| Company name of temperature recording device used                         |   |
| Model of temperature recording device used                                |   |
| Blood pressure recording method used                                      | <input type="checkbox"/> No <input type="checkbox"/> Yes  |
| Type of blood pressure recording method used                              | <input type="checkbox"/> External blood pressure sensor<br><input type="checkbox"/> Implanted blood pressure sensor<br><input type="checkbox"/> Unknown<br><input type="checkbox"/> Other |
| If other, please specify  |   |
| Company name of blood pressure recording device used                      |   |
| Model of blood pressure recording device used                             |   |
| <b>Post-mortem imaging</b>  |   |
| Post-mortem imaging   | <input type="checkbox"/> No <input type="checkbox"/> Yes  |
| If post-mortem imaging was performed, indicate post-mortem delay in hours |   |
| Fixation  | <input type="checkbox"/> No <input type="checkbox"/> Yes  |
| If fixation method was used, specify fixative                             | <input type="checkbox"/> Formalin<br><input type="checkbox"/> Paraformaldehyde<br><input type="checkbox"/> Unknown<br><input type="checkbox"/> Other                                      |
| If other, please specify  |   |

FIGURE 3 (Continued)

important to note that repeated (or high dose) isoflurane anesthesia may alter BBB permeability<sup>17</sup> and may exert antiepileptogenic effects.<sup>24</sup> For example, rats that underwent repeated MR scans using isoflurane (1, 6, and 12 h and 1, 2, and 3 days after paraoxon-induced status epilepticus) had reduced BBB leakage when compared to rats that underwent MR scans using isoflurane once, 48 h after SE.<sup>24</sup>

Two imaging procedures can be used to assess BBB dysfunction: (a) the post-pre semi-quantitative approach during which a T1 or T1-weighted MR scan is made with a relatively long duration (e.g., 10-20 min) before and at a specific time point (typically 10-30 min) after the administration of the contrast agent. Since scanning time is not a limiting factor in this approach, a higher spatial resolution can be achieved ( $125 \mu\text{m}^2/\text{voxel}$ , dependent on the system characterizations); and (b) the dynamic approach during which fast T1 scans (Look-Locker gradient echo MRI, scans last in the order of seconds) are made before, during and after (usually up to 30 min) the infusion of the contrast agent.<sup>25</sup> Due to the natural tradeoff, the fast acquisition results in a lower spatial resolution ( $500 \mu\text{m}^2/\text{voxel}$ ).

The advantage is that both procedures can be used within the same subject and thereby the high spatial resolution of the post-pre approach can be combined with the high temporal resolution of the dynamic approach. Typically, T2-weighted anatomical MR images are also acquired before these approaches, in order to outline regions of interest, identify lesions and perform brain atlas registration.

For the infusion of the contrast agent, two approaches have been reported: a bolus injection during which the contrast agent is given in a relatively short time window (<1 min), leading to a fast rise and subsequent drop in the contrast agent blood concentration during its first passage through the vasculature (“arterial input function” AIF),<sup>26</sup> or a step-down infusion that leads to a fast rise of contrast agent concentration in the blood, which is then maintained at a constant level for the duration of infusion (e.g., 20 min).<sup>25</sup> The step-down infusion has been proposed as a sensitive approach to detect subtle BBB leakage due to prolonged infusion of the contrast agent.<sup>27,28</sup> However, different analysis techniques have been developed to detect both fast and slow kinetics of BBB leakage after single bolus injection (see following text and<sup>29</sup>).

**Parameters**

|  |  |  |  |  |  |  |
|--|--|--|--|--|--|--|
| Imaging date and time                    |  |  |  |  |  |  |
| Time Point after initial insult (days)   |  |  |  |  |  |  |
| Heart Rate (min-max bpm)                 |  |  |  |  |  |  |
| Respiration rate (min-max brpm)          |  |  |  |  |  |  |
| Tidal volume (min-max ml)                |  |  |  |  |  |  |
| Expired O <sub>2</sub> (min-max mm Hg)   |  |  |  |  |  |  |
| Expired CO <sub>2</sub> (min-max mm Hg)  |  |  |  |  |  |  |
| O <sub>2</sub> saturation (min-max %)    |  |  |  |  |  |  |
| Body temperature (min-max °C)            |  |  |  |  |  |  |
| Systolic blood pressure (min-max mm Hg)  |  |  |  |  |  |  |
| Diastolic blood pressure (min-max mm Hg) |  |  |  |  |  |  |

**Instructions:** Please check boxes where applicable. If none of the predetermined options is appropriate use the default space to specify your answer. This form is to be filled in for one individual animal.

FIGURE 3 (Continued)

### 3.3.5 | Analysis and interpretation

Different approaches can be used to analyze CE-MRI data, ranging from a relatively simple visual assessment of enhancement curves to a more complex fitting of data to pharmacokinetic models.<sup>30</sup> BBB permeability to contrast agents can be assessed using the pre-post approach by creating a contrast agent “leakage map,” in which the pre-contrast T1-weighted signal intensity is subtracted from the postcontrast signal intensity and divided by the pre-contrast signal intensity (Figure 4). Typically, a threshold for BBB leakage is set at 20%.<sup>25</sup> In some studies, an upper limit is also set (~100%) to exclude enhancement due to contrast agents within blood vessels.<sup>31</sup> A commonly applied method for the estimation of the rate of vessel-to-tissue leakage ( $K^{trans}$ ) is the Tofts model or its modification by Patlak.<sup>30,32</sup> An alternative approach to measure a slow, subtle leakage has recently been shown by measuring the rate of signal change using linear regression of the signal change 5-15 min after bolus injection. This approach has resulted in the detection of BBB dysfunction in epileptic rats and in human patients with epilepsy.<sup>33</sup> To normalize for inter-individual changes in contrast agent elimination rates, the signal in the sagittal sinus can be used. Bolus injection of gadolinium in epilepsy models has demonstrated acute BBB dysfunction after status epilepticus but often fails to demonstrate persistent leakage,<sup>24,31,34-36</sup>

while a step-down infusion of gadolinium showed persistent BBB dysfunction throughout epileptogenesis.<sup>25,37,38</sup> Interestingly, a recent study demonstrates the suitability of the novel PET tracer [<sup>68</sup>Ga]DTPA, [<sup>99m</sup>Tc]DTPA SPECT, and contrast-enhanced MRI to quantify BBB leakage during early epileptogenesis and indicated that CE-MRI seems to be the most favorable modality due to the highest diagnostic potential.<sup>39</sup> It has been shown that quantitative CE-MRI can also be used in dogs<sup>40</sup> and in humans<sup>29,41-47</sup> with epilepsy, which opens possibilities for future studies to investigate whether BBB imaging can be used for early diagnosis and risk stratification of patients suffering from brain injuries or insults,<sup>17</sup> and to evaluate novel treatments aimed at restoring the BBB.<sup>24,37</sup>

### 3.4 | Angiography

CRF File name: 04 CRF module -Aniography.docx

CDE File name: 04 CDE chart -Aniography.xlsx  
(Supporting information)

#### 3.4.1 | Rationale

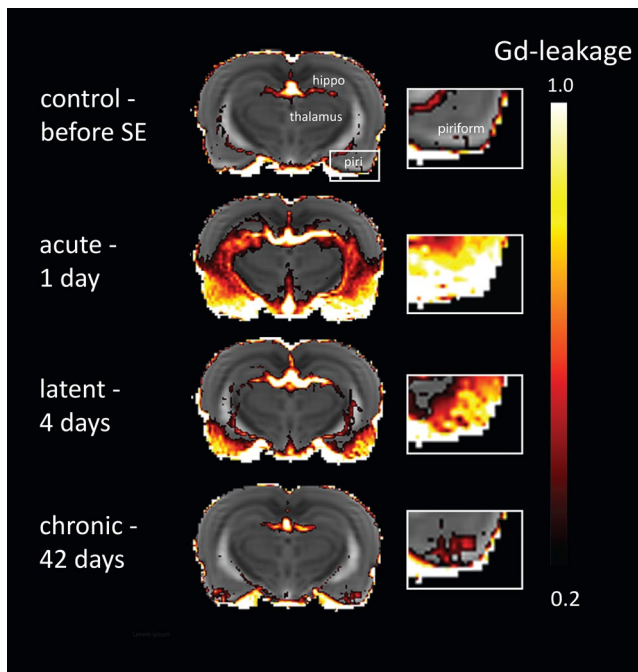
In the current section, we describe two angiography-based approaches to study the cerebral vasculature and perform

TABLE 2 Effects of anesthetics

|                | CBF | CMRO <sub>2</sub> | ICP | AutoReg | CO <sub>2</sub> Reg |
|----------------|-----|-------------------|-----|---------|---------------------|
| Isoflurane     | ↑   | ↓↓                | =/↑ | =/↓     | ↑                   |
| Sevoflurane    | =   | ↓↓                | =   | ↓       | ↑                   |
| Ketamine       | ↑   | =                 | ↑   | ↓       |                     |
| Xylazine       | ↓   | =                 | ↓   | =       | =                   |
| Pentobarbitone | ↓↓  | ↓↓                | ↓↓  | =/↓     | ↓                   |
| Medetomidine   | ↓   | =                 | ↓   | =       | =                   |

Note: Effect: ↓ reduction; ↓↓ strong reduction; ↑ increase; ↑↑ strong increase; =no change. Please note that the effects are influenced by several factors and thus may differ in groups of animals and individual animals. Based on Reimann and Niendorf, *Front Syst Neurosci* 2020, 14:8.

Abbreviations: Autoreg, cerebral autoregulation; CBF, cerebral blood flow; CMRO<sub>2</sub>, cerebral metabolic rate of oxygen consumption; CO<sub>2</sub>Reg, regulation of the CO<sub>2</sub> metabolism; ICP, intracranial pressure.



**FIGURE 4** Blood–brain barrier permeability was assessed after the induction of status epilepticus (SE) in rats using T1-weighted MR images (gradient echo; repetition/echo time, 160/4 ms; flip angle, 70°; acquisition matrix, 256 × 128; voxel resolution, 125 × 125 μm<sup>2</sup>, slice thickness 1.0 mm, that were acquired before and 45 min after the start of a 20 min step-down infusion with Gadolinium (Gd) Using the pre-post approach, “leakage maps” were created, in which the precontrast T1-weighted signal intensity is subtracted from the postcontrast signal intensity and divided by the precontrast signal intensity. A threshold of 20% (0.2) was set. Data acquired by Erwin van Vliet.

quantitative assessment of changes in BBB integrity: the first is a preclinical invasive method, combining high-resolution vasculature imaging with quantitative analysis for the assessment of changes in cerebral blood flow and permeability in anesthetized rats<sup>48–50</sup> (Figure 6); the second is noninvasive CT and MR angiography, which can

be used in rodents and is also used in clinic<sup>51,52</sup> (Figure 7). In the accompanying CRF (see also Figure 8) the most important parameters are described.

### 3.4.2 | Measurements

#### *Direct fluorescent imaging of the cerebrovasculature*

This angiography procedure is conducted in an exposed brain (open-window technique). The method is based on intravenous administration of a fluorescent tracer while imaging dynamic changes of the resultant signal in and surrounding pial (or deeper) vessels. The tracer does not cross the BBB under normal conditions but may do so under pathological conditions (such as epileptic seizures). High-resolution imaging, in time and space, is performed before, during, and after injection of the dye allowing quantitative characterization of dynamic changes in regional blood flow and BBB permeability at the level of single and multiple vessels.<sup>48–50</sup>

### 3.4.3 | Equipment

- Fluorescent microscope equipped with a high-speed camera (e.g., CCD camera).
- Heating pad and pulse oximeter to measure animal body temperature and oxygen saturation
- A standard electrophysiology system for recording neuronal activity (optional).
- Tracer: a low molecular weight tracer such as Sodium fluorescein (MW = 376.3 Da), or the albumin-binding high molecular weight tracer such as Evans blue-albumin (MW = 67 KDa).

- Anesthesia protocols depend on the experimental model and goals of the study (consider the effect of agents on neuronal activity, blood flow, and permeability). Commonly used are intraperitoneal injection of

ketamine (100 mg/ml, 0.08 ml/100 g) and xylazine (20 mg/ml, 0.06 ml/100 g) or continuous inhalation (e.g., oxygen-enriched isoflurane (1-2%).

### 3.4.4 | Procedure

Under deep anesthesia, an intravenous (usually the tail vein) catheter is inserted and the animal's head is fixed in a stereotactic frame. A mid-sagittal incision is performed and the soft tissues are removed from the skull. A cranial window is opened over the selected region of the cerebral cortex. To image pial vessels, the dura can be gently opened and removed, or thinned (until it is transparent). The exposed dura and/or cortex should be continuously superfused with artificial cerebrospinal fluid (aCSF) containing (mM): 124 NaCl, 26 NaHCO<sub>3</sub>, 1.25 NaH<sub>2</sub>PO<sub>4</sub>, 2 MgSO<sub>4</sub>, 2 CaCl<sub>2</sub>, 3 KCl, and 10 glucose, pH 7.4.<sup>48-50,53,54</sup> Recording of brain activity can be

performed in parallel using epidural, subdural, or intracerebral recording electrodes according to the goal of the experiment. For imaging, a BBB nonpermeable tracer (e.g., sodium fluorescein, washout ~30min) is injected intravenously and high-resolution images (~100 μm<sup>2</sup>/pixel) of surface vessels are acquired (≥5 frames/s). To measure permeability, imaging should be started before injection, continue during and last for at least 5 min after the injection (Figure 6B). For the assessment of changes in blood flow and BBB permeability due to seizures, injection of tracer and imaging should be done before and after the induction of an ictogenic agent (applied peripherally or locally such as the potassium channel blocker 4-aminopyridine (4-AP) or the GABA receptor chloride channel blocker picrotoxin (PTX)) (Figure 6A). For repeated measurement of permeability, the injected tracer's half-life in blood should be as short as possible, such that the majority of the tracer has been washed-out prior to subsequent measurements.<sup>49,50</sup>

#### Neuroimaging Studies

Case Report Form: 03 CRF – Contrast-Enhanced Magnetic Resonance Imaging for Blood-Brain Barrier Permeability.docx

CRF module: Contrast-enhanced imaging

Date and time that this CRF was filled out:

Name of person filling out CRF:

Project name/Identifier:

Animal ID:

| CDE Name  | Data Collected   |
|---|--|
| <b>Imaging sequence</b>   |  |
| Quantitative or weighted images                                 | <input type="checkbox"/> Quantitative map <input type="checkbox"/> Contrast-weighted<br><input type="checkbox"/> Unknown   |
| Sequence  | <input type="checkbox"/> Fast spin echo <input type="checkbox"/> Gradient echo <input type="checkbox"/> Spoiled GRE<br><input type="checkbox"/> Steady state GRE <input type="checkbox"/> Look-Locker GRE<br><input type="checkbox"/> Angiography <input type="checkbox"/> Unknown |
| Specify the sequence / sequence name                            |  |
| Dimensions  | <input type="checkbox"/> 2D <input type="checkbox"/> 3D <input type="checkbox"/> Unknown   |
| Isotropic resolution  | <input type="checkbox"/> Yes <input type="checkbox"/> No <input type="checkbox"/> Unknown  |
| Resolution in mm  | _____ x _____ x _____  |
| Coverage (FOV coverage)   | <input type="checkbox"/> Whole brain <input type="checkbox"/> Cerebrum <input type="checkbox"/> Partial coverage<br><input type="checkbox"/> Unknown   |
| Contrast  | <input type="checkbox"/> T1-weighted <input type="checkbox"/> Fluid-attenuated <input type="checkbox"/> T2-weighted<br><input type="checkbox"/> Unknown  |
| <b>Imaging parameters</b>                                       |  |
| Repetition time (TR) in ms                                      |  |
| Flip angle in degrees   |  |
| Echo time (TE) / Effective echo time (TE <sub>eff</sub> ) in ms |  |
| Base echo time in ms  |  |

FIGURE 5 Contrast-enhanced imaging case report form (see main text for details)

|  |   |
|--|---|
| Echo spacing in ms                                     |   |
| Number of echoes                                       |   |
| Otherwise: specify echo train in ms                    |   |
| Inversion time (inversion recovery T1) in ms           |   |
| Specify array (inversion time array) in ms             |   |
| k-space coverage / encoding                            |   |
| Partially parallel imaging acceleration                |   |
| Partial-FT acceleration (1 if no acceleration)         |   |
| Zero-fill acceleration (1 if no acceleration)          |   |
| Other acceleration method                              |   |
| Read direction   | <input type="checkbox"/> S-I (superior-inferior) <input type="checkbox"/> L-R (left-right)<br><input type="checkbox"/> H-F (head-feet) <input type="checkbox"/> Unknown   |
| <b>Baseline image</b>                                  |   |
| Baseline image before any contrast agent               | <input type="checkbox"/> Yes <input type="checkbox"/> No <input type="checkbox"/> Unknown   |
| <b>Contrast agent</b>                                  |   |
| Contrast agent used                                    | <input type="checkbox"/> None<br><input type="checkbox"/> Gadolinium-DTPA<br><input type="checkbox"/> Ultrasmall SuperParamagnetic Iron Oxide<br><input type="checkbox"/> Unknown<br><input type="checkbox"/> Other |
| If other, please specify                               |   |
| Name of contrast agent                                 |   |
| Manufacturer of contrast agent                         |   |
| Route of administration contrast agent                 | <input type="checkbox"/> Intravenous<br><input type="checkbox"/> Intra-articular  |
| Dose contrast agent used in mg/kg                      |   |
| Administration contrast agent                          | <input type="checkbox"/> Bolus injection<br><input type="checkbox"/> Infusion   |
| Infusion rate contrast agent in ml/min                 |   |
| Scan time point(s) after contrast agent administration |   |

**Parameters**

|  |  |  |  |  |  |  |
|--|--|--|--|--|--|--|
| Imaging date and time                  |  |  |  |  |  |  |
| Time Point after initial insult (days) |  |  |  |  |  |  |

**Instructions:** Please check boxes where applicable. If none of the predetermined options is appropriate use the default space to specify your answer. This form is to be filled in for one individual animal.

FIGURE 5 (Continued)

3.4.5 | Analysis and interpretation

Image analysis includes subpixel image registration, segmentation using noise filtration, hole-filling, and adaptive threshold to produce a binary image, separating blood vessels from extravascular regions. Pixel-wise signal intensity changes over time are calculated (intensity vs time, IT) for arteriole, venous, and extravascular compartments.<sup>48-50</sup> A BBB permeability index (PI) is calculated for each extravascular pixel as the ratio between the IT curve

and the arteriole's curve based on the late period after injection.<sup>48-50</sup> Fitting a PI to each extravascular pixel enables spatial mapping of BBB permeability (Figure 6C).

Magnetic resonance angiography (MRA)

Noninvasive angiography approaches, such as CT and MR-angiography (MRA), are based on the injection of contrast agent (commonly Gd-based) for accurate imaging of

cerebral vasculature. These methodologies are commonly used in the clinic for the detection of cerebrovascular pathologies such as aneurysms, stroke, and stenosis.<sup>51,52,55,56</sup> Although it is not one of the prevalent neuroimaging techniques of epilepsy, MRA can be performed in epileptic patients (alongside other MRI sequences) for the detection of disturbed vasculature in and surrounding the epileptogenic focus in high spatial resolution.<sup>57</sup>

### 3.4.6 | Equipment

Magnetic resonance angiography requires high spatial resolutions and therefore benefits from the use of anatomically shaped surface-receive coils and phased-array technology in order to increase signal-to-noise ratios.

### 3.4.7 | Procedure

Two different methods for performing MRA are the time of flight (TOF, [Figure 7](#)) and phase contrast angiography (PCA) while methods such as Fourier Velocity Encoding (FVE) allow mapping the average blood velocities inside the vessels. TOF angiography utilizes short TRs and a relatively large flip angle to saturate the surrounding stationary tissues while blood flowing into the imaging plane has “fresh” nonsaturated protons and therefore appears hyperintense.

For 2D TOF, a large number of thin slices (~250  $\mu\text{m}$ ) to cover the whole FOV can be acquired with high flip angles (>75 degrees). For 3D, comparatively smaller flip angles (~20 degrees) are used to avoid saturation of moving spins in the FOV and hence have typically lower vessel/tissue contrast. High resolutions can be acquired with partial k-space where necessary to reduce scan times. Importantly, for 2D acquisitions, blood in vessels running parallel to the slice plane can be subjected to multiple excitation pulses and therefore lose contrast. The same is true for slow-moving blood flowing through the FOV in 3D acquisitions.

Phase contrast angiography uses bipolar flow-encoding gradients to encode protons in the tissue of interest. Stationary tissue spins undergo equivalent phase shifts with each forward and reversed gradient and therefore cancel out, while moving spins within the blood vessels have a residual phase angle depending on their velocity in the direction of the applied gradients.

### 3.4.8 | Analysis and interpretation

MRA images are typically analyzed and interpreted qualitatively using maximum intensity projections (MIPs).

While this improves contrast between vessels and tissue, it is important to keep in mind that resolution is decreased in the process.

## 3.5 | Arterial spin labeling

CRF File name: 05 CRF module - Arterial spin labeling.docx

CDE File name: 05 CDE chart -Arterial Spin Labeling.xlsx ([Supporting information](#))

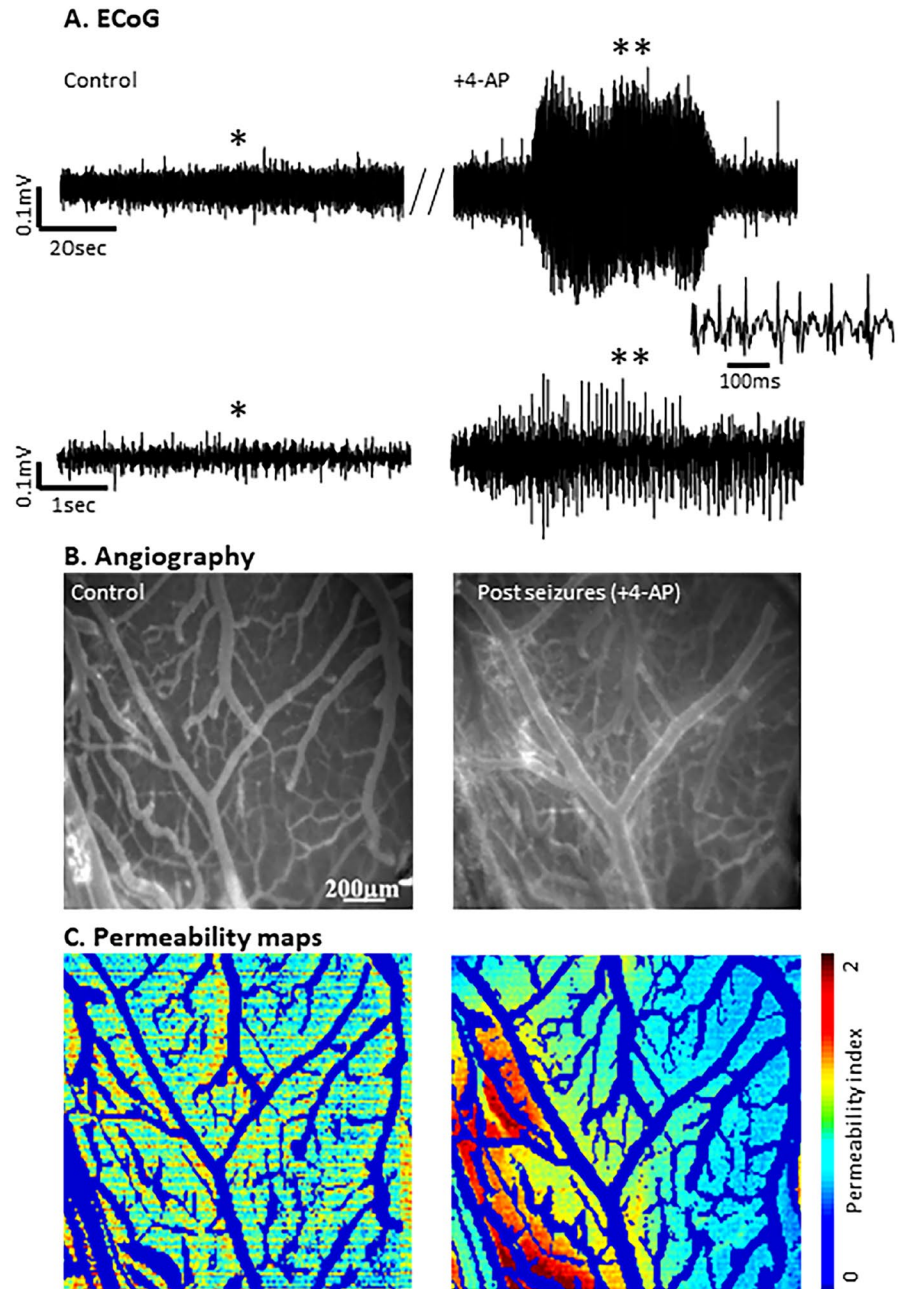
### 3.5.1 | Rationale

Arterial Spin Labeling (ASL) is a completely noninvasive approach for quantitative measurement of cerebral blood flow (CBF) using endogenous contrast from blood flowing into the brain. The pulse sequence is based upon magnetically labeling hydrogen in water within inflowing blood using radiofrequency pulses. As CBF is closely linked with metabolism and neural function, it is one of the key parameters defining the state of the tissue. In epilepsy patients, ASL is used to characterize CBF in the ictal and interictal state and to localize the epileptic focus.<sup>58</sup> In preclinical settings, ASL has been used to assess the contribution of compromised CBF to hippocampal damage in the rat pilocarpine status epilepticus model,<sup>59</sup> and to follow CBF changes over time in the rat post-traumatic epilepsy model ([Figure 9](#)).<sup>60</sup> In this section and in the accompanying CRF (see also [Figure 10](#)), we describe the most important parameters for ASL.

### 3.5.2 | Measurements

There are multiple variants of ASL. As a general rule, pulsed ASL (PASL) techniques based on subtraction of slice selective vs. global inversion, such as flow alternated inversion recovery (FAIR),<sup>61</sup> works well for mice, when the volume/transmit radiofrequency coil covers most of the animal for efficient global inversion. Continuous ASL (CASL, or pseudocontinuous PCASL) with a radiofrequency-saturation band in the neck and control measurements with a saturation band outside of the head at the opposite side of the imaging slice are used for rat. A long radiofrequency pulse with a slice selective gradient causes flow-driven adiabatic inversion for inflowing spins only if B1 of the saturation is high enough to maintain adiabatic conditions. Therefore, careful B1 calibration and validation of the inversion efficiency are key steps in the implementation, especially as the neck is often in the peripheral area of the volume/transmit coil, which may behave suboptimally. Alternatively, a separate tagging coil

**FIGURE 6** Fluorescent angiography to study BBB integrity. (A) Following craniotomy, electrocorticography (ECoG) is recorded, and seizures are induced using 4-AP. (B) The BBB nonpermeable tracer sodium fluorescein is injected intravenously and simultaneously high-frequency images of pial vessels are repeatedly obtained before (control) and following 4-AP-induced seizures. (C) Permeability maps, before (left) and following seizures (right). Warm colors over the extravascular regions indicate BBB dysfunction. Data acquired by Ofer Prager and Alon Friedman.



for the neck is recommended in preclinical experiments; however, this requires additional hardware. Background suppression is recommended for better contrast to noise.<sup>62</sup> The ASL signal increases with label duration; however, the optimum is typically reached with a labeling duration that is shorter than  $T_1$  of blood in the given field strength, as labeling duration also affects TR. Postlabeling delay is another important parameter requiring optimization and the optimal delay depends on multiple issues including anesthesia and field strength, that influence basal CBF and  $T_1$ , respectively. If the delay time is too short, it does not allow enough delivery of the labeled blood to the tissue, while if it is too long, poor signal-to-noise occurs due to  $T_1$  decay.<sup>62</sup> As a readout imaging sequence, both fast

spin echo and EPI-type sequences can be used. 3D sequences are recommendable over 2D sequences. FSE (or segmented EPI) results in less image distortion and is typically used when more time can be used to obtain higher quality data, while (single shot) EPI is used for dynamic studies. As a control, B1 map should be acquired as labeling efficiency is dependent on B1.

### 3.5.3 | Equipment

Arterial Spin Labeling benefits from a high magnetic field more than most other MRI techniques as  $T_1$  is field dependent and longer  $T_1$  at a higher field increases the lifetime of

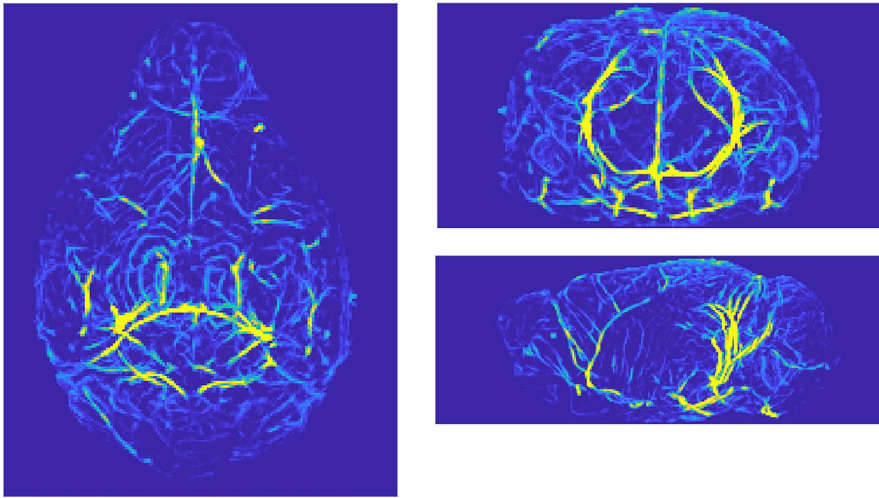


**FIGURE 7** Magnetic resonance angiography in a mouse brain. Time of flight (TOF) images were acquired at 9.4T using a 4-channel receive only cryocoil in ~5 min with an isotropic spatial resolution of  $75 \mu\text{m}^3$ . Vessel enhancement filtering<sup>151,152</sup> and maximum intensity projections were reconstructed using MATLAB. Data acquired by David Wright.

### Neuroimaging Studies

Case Report Form: 04 CRF Module – angiography.docx

CRF module: Angiography

Date and time that this CRF was filled out:

Name of person filling out CRF:

Project name/Identifier:

Animal ID:

| <u>CDE Name</u>          | <u>Data Collected</u>  |
|--------------------------|--|
| <b>Angiography</b>       |  |
| Cranial window           | <input type="checkbox"/> Open window <input type="checkbox"/> Closed window <input type="checkbox"/> Unknown   |
| Imaging protocol         |  |
| Duration                 | <input type="checkbox"/> 306s <input type="checkbox"/> Unknown <input type="checkbox"/> Other  |
| If other, please specify |  |
| Frame rate               | <input type="checkbox"/> 5/s <input type="checkbox"/> Unknown <input type="checkbox"/> Other   |
| If other, please specify |  |
| Magnification            | <input type="checkbox"/> x30, <input type="checkbox"/> x40, <input type="checkbox"/> Unknown <input type="checkbox"/> Other  |
| If other, please specify |  |
| Name of tracer           | <input type="checkbox"/> Sodium Fluorescein (MW=376.3 g/mol)<br><input type="checkbox"/> Lucifer Yellow (MW=442.3 g/mol)<br><input type="checkbox"/> Evans Blue (MW <sub>free</sub> =960.8g/mol<br>MW <sub>Albumin</sub> =67kg/mol,)<br><input type="checkbox"/> Other |
| If other, please specify |  |
| Wavelength               | <input type="checkbox"/> 488 nm <input type="checkbox"/> 595 nm <input type="checkbox"/> Unknown <input type="checkbox"/> Other  |
| If other, please specify |  |

**FIGURE 8** Angiography case report form (see main text for details)

the labeling. A large, efficient transmit coil is required to enable global inversion at the level of the heart or flow-driven adiabatic inversion at the level of the neck. Alternatively, a separate tagging coil in a different channel can be used.

MRI-compatible equipment for extensive physiological monitoring and mechanical ventilation are needed as CBF depends on temperature, CO<sub>2</sub> level, and anesthesia (type and depth) (see Physiological monitoring for details).

|  |   |
|--|---|
| Route of administration                                    | <input type="checkbox"/> Intravenous (bolus) <input type="checkbox"/> Unknown <input type="checkbox"/> Other  |
| If other, please specify                                   |   |
| Dose in mg/kg  |   |
| <b>Time of Flight (TOF) Magnetic Resonance Angiography</b> |   |
| Geometry   | <input type="checkbox"/> 3D<br><input type="checkbox"/> 2D multi-slice<br><input type="checkbox"/> Unknown  |
| Flip Angle in degrees                                      |   |
| Flow Saturation  | <input type="checkbox"/> No <input type="checkbox"/> Yes <input type="checkbox"/> Unknown   |
| If yes, please specify direction                           | <input type="checkbox"/> Rostral <input type="checkbox"/> Caudal <input type="checkbox"/> Unknown   |
| Distance in mm   |   |
| Thickness in mm  |   |
| <b>Phase Contrast Angiography (PCA)</b>                    |   |
| Geometry   | <input type="checkbox"/> 3D <input type="checkbox"/> 2D multi-slice <input type="checkbox"/> Unknown  |
| Flip Angle in degrees                                      |   |
| Phase contrast direction                                   | <input type="checkbox"/> All <input type="checkbox"/> Read <input type="checkbox"/> Slice <input type="checkbox"/> Phase <input type="checkbox"/> Unknown |
| Estimated Maximum Flow Velocity in cm/s                    |   |
| Twister Gradient   | <input type="checkbox"/> No <input type="checkbox"/> Yes <input type="checkbox"/> Unknown   |

**Parameters**

|  |  |  |  |  |  |  |
|--|--|--|--|--|--|--|
| Imaging date and time                  |  |  |  |  |  |  |
| Time Point after initial insult (days) |  |  |  |  |  |  |

**Instructions:** Please check boxes where applicable. If none of the predetermined options is appropriate use the default space to specify your answer. This form is to be filled in for one individual animal.

FIGURE 8 (Continued)

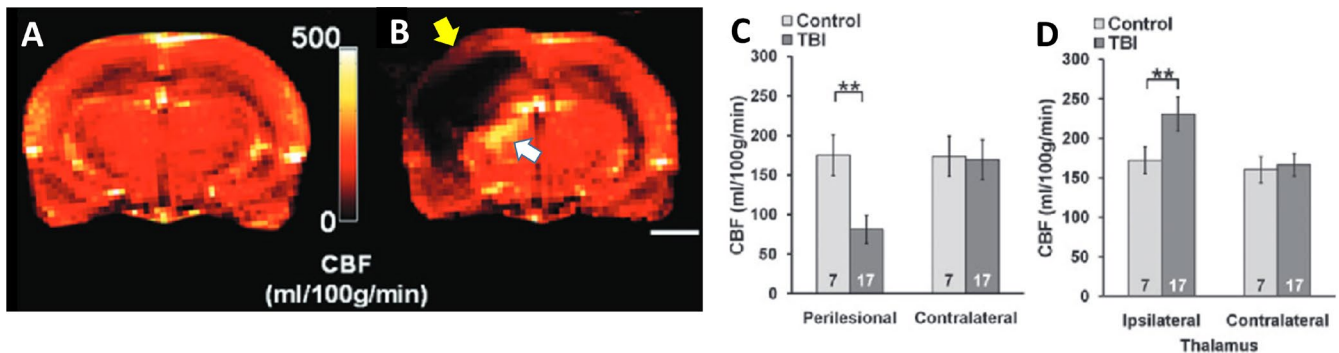


FIGURE 9 Cerebral blood flow maps acquired with continuous arterial spin labeling (CASL) from sham-operated (A) or traumatic brain injury (B) rats at 8 months after induction of lateral fluid percussion induced injury. The yellow arrow indicates a hypoperfused area within the perilesional cortex, and the white on the image indicates a hyperperfused area of thalamus. Quantification of the CBF in corresponding ipsilateral and contralateral areas (C, D). Figure reproduced with modifications from <sup>153</sup> with permission of Mary Ann Liebert, Inc.

3.5.4 | Procedure

Arterial Spin Labeling is typically performed in anesthetized animals. The depth and type of anesthesia have a direct influence on CBF and there is currently no agreement in the field regarding the best anesthesia for pre-clinical ASL studies. Animals under isoflurane anesthesia have abnormally high basal CBF while animals under

medetomidine sedation have lower than normal CBF.<sup>63</sup> CBF in combination with medetomidine and isoflurane, or with urethane anesthesia is closer to normal. In all cases, careful monitoring of physiological parameters is required as, for example, CO<sub>2</sub> is a vasodilator with direct effects on cerebral blood volume and CBF. With most anesthetics, mechanical ventilation is required to maintain normal CO<sub>2</sub> levels. If preparatory surgery is performed,

**Neuroimaging Studies****Case Report Form: 05 CRF- Arterial spin labeling.docx****CRF module: Arterial spin labeling**Date and time that this CRF was filled out:Name of person filling out CRF:Project name/Identifier:Animal ID:

| <u>CDE Name</u>                     | <u>Data Collected</u>  |
|-------------------------------------|--|
| <b>Arterial spin labeling (ASL)</b> |  |
| ASL imaging method                  | <input type="checkbox"/> continuous ASL (CASL)<br><input type="checkbox"/> pseudo-continuous ASL<br><input type="checkbox"/> pulsed ASL (PASL)<br><input type="checkbox"/> Unknown<br><input type="checkbox"/> Other |
| If other, please specify            |  |
| Specify sequence name               |  |
| <b>Radiofrequency coil</b>          |  |
| Separate labeling coil              | <input type="checkbox"/> Yes <input type="checkbox"/> No <input type="checkbox"/> Unknown  |
| Volume coil as labeling coil        | <input type="checkbox"/> Yes <input type="checkbox"/> No <input type="checkbox"/> Unknown  |
| Dimensions of the volume coil in cm |  |
| <b>Labeling pulse</b>               |  |
| Pulse shape                         |  |
| Pulse duration in ms                |  |
| Pulse bandwidth in kHz              |  |
| Pulse power in kW                   |  |
| Location                            | <input type="checkbox"/> Neck <input type="checkbox"/> Other <input type="checkbox"/> Unknown  |
| If other please specify             |  |
| Labeling slab thickness in mm       |  |

**FIGURE 10** Arterial spin-labeling case report form (see main text for details)

time spent under isoflurane anesthesia and the time between cessation of isoflurane anesthesia and the beginning of ASL should be kept constant and documented. Special attention should be paid for fixing the animal's head using ear bars and a tooth bar, as ASL is a subtraction technique and therefore inherently very sensitive to movement. Probes for physiological monitoring are attached to the animal and the animal is inserted into the magnet bore for ASL measurements. Physiological monitoring is performed continuously and values are recorded. Blood gases should be analyzed at least once during the experiment but preferably at the beginning and at the end of the ASL scan.

### 3.5.5 | Analysis and interpretation

ASL allows for quantitative CBF and therefore is well suited for longitudinal studies or multicenter studies. The values needed for calculation include blood T1, partition coefficient, and labeling efficiency.

## 3.6 | Diffusion-weighted magnetic resonance imaging

CRF File name: 06 CRF module - Diffusion-weighted imaging.docx

CDE File name: 06 CDE chart - Diffusion-weighted imaging.xlsx ([Supporting information](#))

### 3.6.1 | Rationale

Diffusion-weighted imaging (DWI) exploits the microscopic Brownian motion of water molecules as they diffuse through tissues of interest. Contrast is generated as the water is obstructed or restricted by cell membranes, neurites, and macromolecules, and as such, DWI is sensitive to microstructural changes to the tissue that can be invisible to conventional structural imaging techniques ([Figure 11](#)). The raw data are conventionally fit to the diffusion tensor construct from which numerous indices are derived to report on local tissue microstructure. These include fractional

|   |   |
|---|---|
| Inversion time (TI) in ms                                     |   |
| Post labeling delay in ms                                     |   |
| Control image: control slab location                          |   |
| Number of label-control image pairs acquired                  |   |
| T1 map acquired   | <input type="checkbox"/> Yes <input type="checkbox"/> No <input type="checkbox"/> Unknown |
| <b>Imaging parameters</b>                                     |   |
| Dimension   | <input type="checkbox"/> 2D <input type="checkbox"/> 3D <input type="checkbox"/> Unknown  |
| Number of slices (1 if 3D)                                    |   |
| Slice thickness / slab thickness in mm                        |   |
| Slice gap in mm   |   |
| FOV in mm   | _____ x _____ x _____   |
| Matrix / number of points                                     | _____ x _____ x _____   |
| Repetition time (TR) in ms                                    |   |
| Echo time (TE) in ms  |   |
| <b>Assumptions for CBF calculations</b>                       |   |
| Constant T1 assumed:  | <input type="checkbox"/> Yes <input type="checkbox"/> No <input type="checkbox"/> Unknown |
| Partition coefficient / blood tissue distribution coefficient |   |
| Movement correction applied                                   | <input type="checkbox"/> Yes <input type="checkbox"/> No <input type="checkbox"/> Unknown |
| Other details   |   |
| Analysis pipeline   |   |

**Parameters**

|  |  |  |  |  |  |  |
|--|--|--|--|--|--|--|
| Imaging date and time                  |  |  |  |  |  |  |
| Time Point after initial insult (days) |  |  |  |  |  |  |

**Instructions:** Please check boxes where applicable. If none of the predetermined options is appropriate use the default space to specify your answer.  
This form is to be filled in for one individual animal.

**FIGURE 10** (Continued)

anisotropy, axial (parallel) diffusivity, radial (diffusivity), and mean diffusivity among others. Alternatively, or in addition, extended or multi-shell data can be fit to various diffusion models to derive indices that may reflect more detailed structural changes related to extra and intracellular compartments. The numerous parametric indices derived from DWI datasets can provide information about various pathologies related chiefly to microstructural changes, status of myelination, cellular edema, and structural connectivity. DWI has been usefully employed in preclinical epilepsy research models.<sup>64–67</sup> In this section and in the accompanying CRF (see also [Figure 12](#)), we provide the minimal framework for parameter reporting that would be required for joint analysis of data acquired from multiple sites.

### 3.6.2 | Measurements

For in vivo imaging in rodents, echo-planar imaging (EPI)-based acquisitions with isotropic resolutions are

preferred. The FOV should be orientated in the axial orientation (i.e., with the slice, or second phase-encode, direction orientated superior-inferior) as this requires the fewest slices/phase-encode steps, when imaging rodents and therefore minimizes the total scan time. Fat suppression should be on, and where necessary, outer-volume saturation can be employed to reduce the field of view. This has the advantage of reducing the required matrix size to achieve a given resolution and therefore ultimately reduces the minimum echo time required.

Two of the most important parameters to set are the maximum b-value(s) and the number of diffusion directions. The reconstruction of white matter fibers orientation and intra-axonal water diffusion requires both a sufficiently high b-value and a sufficient number of uniformly distributed diffusion directions. However, high b-values necessitate longer diffusion gradients, which increase TE and reduce the signal-to-noise ratio. While TE can be reduced by acquiring multiple shots, both the number of shots and the number of required diffusion directions both impact on the total

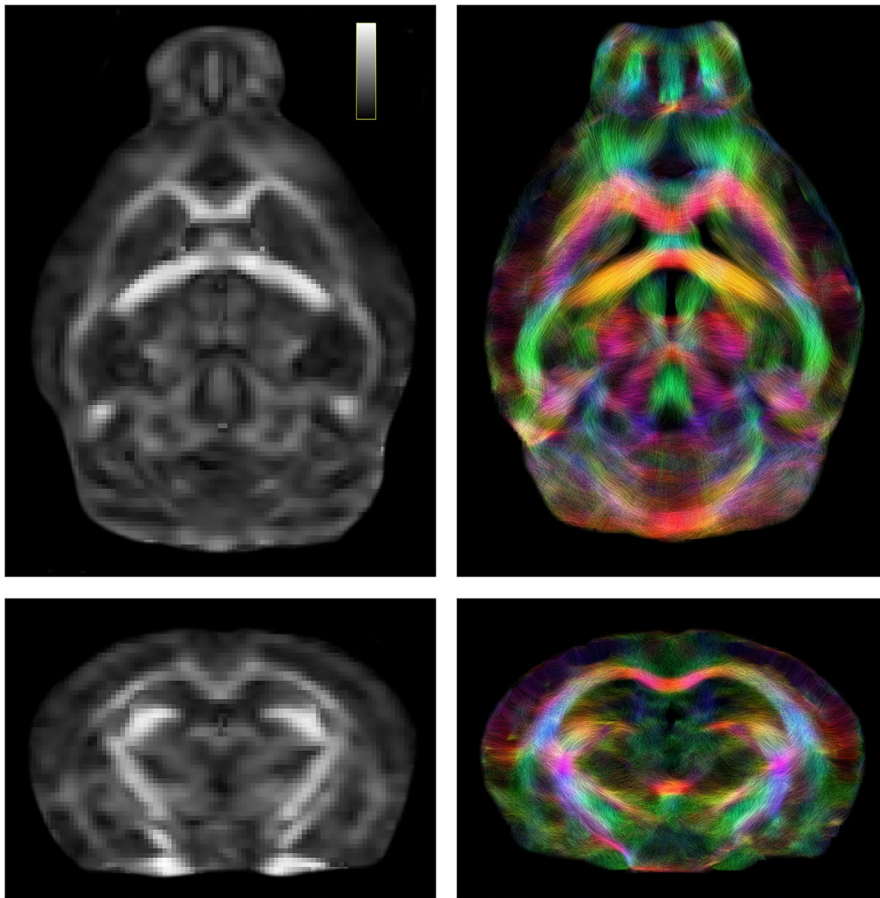


**FIGURE 11** Diffusion-weighted imaging (DWI) in the adult mouse brain. Example fractional anisotropy (FA, left column) and tractography images (right column) acquired in vivo at 9.4 T using a single-channel, anatomically shaped surface coil. Two diffusion shells ( $b$ -values = 1500 and 3000 s/mm<sup>2</sup>) with 81 directions were acquired at 250  $\mu$ m isotropic resolution in <10 min. DWIs were upsampled to 125  $\mu$ m isotropic resolution, and FA and tractography images were reconstructed using MRtrix3 software. Color bar shows FA values from 0 (black) to 1 (white). Tractography streamlines are color-encoded according to orientation: red, medial-lateral; green, anterior-posterior; and blue, superior-inferior. Data acquired by David Wright.

scan time. For in vivo rodent imaging, a  $b$ -value of 3000 s/mm<sup>2</sup> and 60 diffusion directions are recommended. If more time is available, a second, lower  $b$ -value can be added (e.g.,  $b$ -value = 1500 s/mm<sup>2</sup>) or additional diffusion directions can be acquired. In order to improve data consistency and to facilitate collaboration across multiple centers, there is a need for reporting  $b$ -values and making vectors available since not only are the derived quantitative indices  $b$ -value dependent,<sup>68</sup> mono-exponential signal fitting is invalid at very high  $b$ -values, and would require careful processing to obtain accurate values.

Apart from B0 field strength and shim homogeneity, the variability in gradient performance and stability at different sites is the biggest single factor that may determine whether multi-site data can be credibly pooled. Indeed, the least capable gradient system among different sites becomes the lowest common denominator for determining the type of sequence used (e.g., 2- vs 3-dimensional image acquisition, the number of slices, TE, matrix size,  $b$ -value and the duration of the diffusion gradient (so-called “little delta”), as well as the time between diffusion-sensitizing gradients (so-called “Big Delta”), of which the latter will affect the specific amplitude of diffusion that the diffusion sequence is sensitive to). Careful and thorough reporting of these parameters should go a long way to facilitate successful multi-site collaborations.

### 3.6.3 | Equipment

As outlined in the notes above, gradient performance and stability are of paramount importance. For quantitative analysis of diffusion, images must be acquired over multiple diffusion gradients and often, with multiple  $b$ -values (shells). Although the diffusion tensor can be estimated using six directions, for a rotationally-invariant DTI reconstruction, 30 uniformly distributed, noncolinear vectors are needed, with over 45 required for characterizing fiber orientation distributions (FODs).<sup>69</sup> This need for large numbers of imaging shells necessitates rapid image acquisitions, typically EPI-based, which benefit from high-powered gradients with short rise times.

Sequence optimization requires that diffusion times are long enough to ensure that water molecules interact with the boundaries of the tissue of interest and with sufficient diffusion weighting to increase the angular diffusion profile sharpness and fiber orientation specificity. Together with a requirement for sufficiently high isotropic resolution, these factors combine to increase echo times and decrease the signal-to-noise ratio. As such, and similar to other neuroimaging techniques, DWI benefits from the use of anatomically shaped surface-receive coils and phased-array technology and

**Neuroimaging Studies****Case Report Form: 06 CRF - Diffusion-weighted imaging.docx****CRF module: Diffusion-Weighted Imaging**Date and time that this CRF was filled out:Name of person filling out CRF:Project name/Identifier:Animal ID:

| <u>CDE Name</u>                         | <u>Data Collected</u>  |
|---|--|
| <b>Diffusion weighted imaging (DWI)</b> |  |
| Imaging sequence                        | <input type="checkbox"/> Echo Planar Imaging<br><input type="checkbox"/> Spin-Echo <input type="checkbox"/> Unknown                                  |
| <b>Imaging Parameters</b>               |  |
| Dimension                               | <input type="checkbox"/> 2D <input type="checkbox"/> 3D <input type="checkbox"/> Unknown   |
| Isotropic resolution                    | <input type="checkbox"/> Yes <input type="checkbox"/> No <input type="checkbox"/> Unknown  |
| Resolution in mm                        | _____ x _____ x _____  |
| Coverage (FOV coverage)                 | <input type="checkbox"/> Whole brain <input type="checkbox"/> Cerebrum <input type="checkbox"/> Partial coverage<br><input type="checkbox"/> Unknown |
| Segmented / single shot acquisition     | <input type="checkbox"/> Single shot <input type="checkbox"/> Segmented <input type="checkbox"/> Spiral <input type="checkbox"/> Unknown             |
| Number of segments                      |  |
| Repetition time (TR) in ms              |  |
| Echo time (TE) in ms                    |  |
| EPI echo spacing in ms                  |  |
| Spectral width in kHz                   |  |
| <b>k-space coverage / encoding</b>      |  |
| Partially parallel imaging acceleration | <input type="checkbox"/> Yes <input type="checkbox"/> No <input type="checkbox"/> Unknown  |
| Partial-FT acceleration                 | <input type="checkbox"/> Yes <input type="checkbox"/> No <input type="checkbox"/> Unknown  |
| Zero-filled acceleration                | <input type="checkbox"/> Yes <input type="checkbox"/> No <input type="checkbox"/> Unknown  |

**FIGURE 12** Diffusion-weighted imaging case report form (see main text for details)

order to either/both increase signal-to-noise and reduce acquisition times.

### 3.6.4 | Procedure

After induction of anesthesia, the rodent is securely fixed with a 3-point stereotaxic-like cradle, which is important to prevent head movement that will result in image ghosting or at least signal deviations that affect the calculation of the final indices. Mice can have labored, gasping respiration that can be alleviated by a slower anesthetic induction with isoflurane or using a different sedation agent. Gating the acquisition to respiration does improve image quality, but at the expense of significantly prolonged imaging time, variable TR values, and increased exposure to anesthetic. The recommendation is to avoid gating and use the extra time to acquire images along more gradient vectors and use a priori-defined criterion to determine

those scans that should be removed for excessive head motion. Correction of phase distortion due to locally adjacent air/bone/brain at the ears and the thick frontal bones can be somewhat corrected by acquiring a reverse phase-encode b0 image and then processing the data with FSL's *Topup*.<sup>70</sup>

### 3.6.5 | Analysis and interpretation

A number of freely available software tools have been developed for processing DWI, each with its own unique methodologies. However, there are a number of universal preprocessing steps that should be undertaken irrespective of the tool used:

- Denoising and Gibbs ringing removal
- Motion correction either at the slice or at least the volume level.

|   |   |
|---|---|
| Other acceleration method                                     |   |
| Read direction  | <input type="checkbox"/> S-I (superior-inferior) <input type="checkbox"/> L-R (left-right)<br><input type="checkbox"/> H-F (head-feet) <input type="checkbox"/> Unknown |
| Phase1 direction  | <input type="checkbox"/> S-I (superior-inferior) <input type="checkbox"/> L-R (left-right)<br><input type="checkbox"/> H-F (head-feet) <input type="checkbox"/> Unknown |
| Respiration gating  | <input type="checkbox"/> Yes <input type="checkbox"/> No <input type="checkbox"/> Unknown   |
| Reverse phase encode acquisition                              | <input type="checkbox"/> Yes <input type="checkbox"/> No <input type="checkbox"/> Unknown   |
| Fat suppression   | <input type="checkbox"/> Yes <input type="checkbox"/> No <input type="checkbox"/> Unknown   |
| Outer volume suppression                                      | <input type="checkbox"/> Yes <input type="checkbox"/> No <input type="checkbox"/> Unknown   |
| <b>Diffusion Parameters</b>                                   |   |
| Diffusion gradient duration ( $\delta$ ) in ms                |   |
| Diffusion gradient separation ( $\Delta$ ) in ms              |   |
| Number of b-values (no of shells)                             |   |
| Number of Directions @ b-value (shell 1) in s/mm <sup>2</sup> |   |
| Number of Directions @ b-value (shell 2) in s/mm <sup>2</sup> |   |
| Number of Directions @ b-value (shell 3) in s/mm <sup>2</sup> |   |
| <i>(Insert additional rows for each shell)</i>                | <i>(Insert additional rows for each shell)</i>  |
| Number of Non-Diffusion Images (b <sub>0</sub> images)        |   |

**Parameters**

|   |  |  |  |  |  |  |
|---|--|--|--|--|--|--|
| Imaging date and time                   |  |  |  |  |  |  |
| Time Point after initial insults (days) |  |  |  |  |  |  |

**Instructions:** Please check boxes where applicable. If none of the predetermined options is appropriate use the default space to specify your answer.  
This form is to be filled in for one individual animal.

FIGURE 12 (Continued)

- Distortion correction, including eddy-current distortion correction (typically performed in one step)
- B1 field inhomogeneity correction
- Outlier detection of vector images with signal abnormalities

Although voxel-based statistics are most suited to an unbiased analysis, where a priori hypothesis testing necessitates a restricted regional analysis, for example, to directly compare MRI connectomic data to EEG data within the same animals, then an analysis using a region-of-interest approach would be expected to be the most appropriate methodology.

**3.7 | Volumetry**

CRF File name: 07 CRF module—Volumetry.docx

CDE File name: 07 CDE chart—Volumetry.xlsx  
([Supporting information](#))

**3.7.1 | Rationale**

Anatomical MR imaging assesses: (a) the lesion size, location, and structural changes due to the initial insult launching the epileptogenic processes, and (b) the progressive atrophy during the epileptogenesis and epilepsy, which is commonly included in preclinical imaging studies. Anatomical information on ventricular enlargement or local atrophy and major volumetric changes is necessary for the correct analysis of data from other imaging modalities, e.g., PET. Moreover, the volumetric information extracted describes tissue atrophy, swelling, cortical thinning etc. that are features both relevant as comorbidities and potentially reflecting epileptogenic processes.<sup>71–74</sup>

## Acute edema, hemorrhagic lesion and progressive atrophy

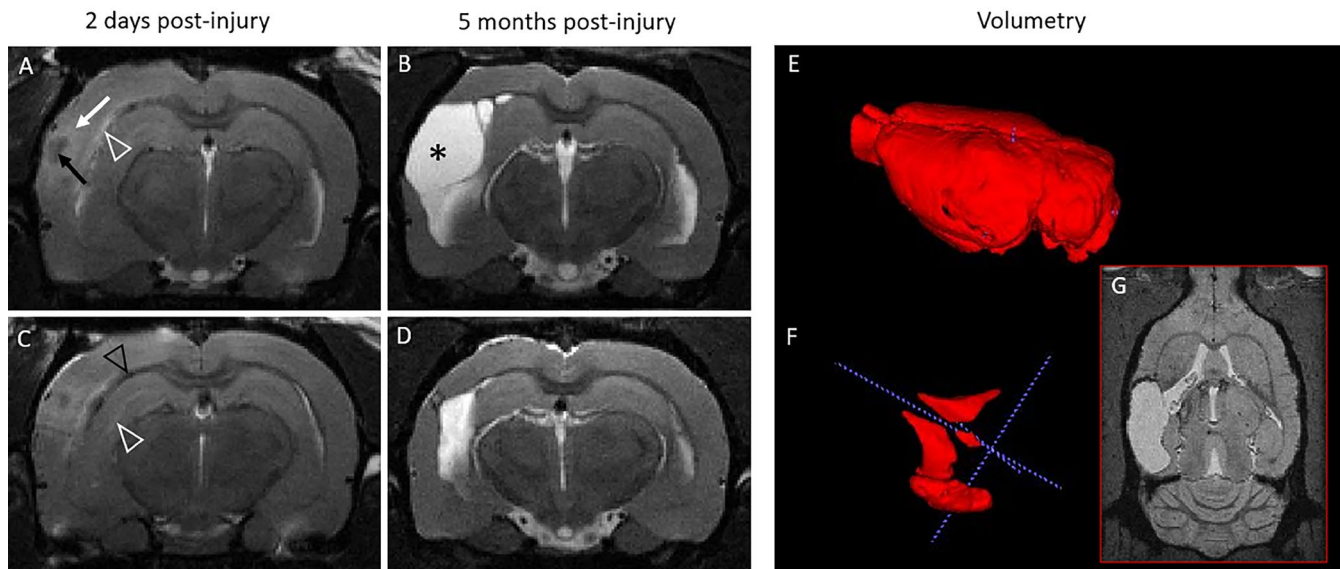


**FIGURE 13** T2-weighted images of the lateral fluid percussion injury rat model of post-traumatic epilepsy in the acute and chronic stages. Two representative animals (A and C) shown 2 days postinjury, and 5 months later (B and D). T2-weighted images show the acute edema in the cortex (white arrow in A), along white matter tracts (arrowhead in A), and in the hippocampus (white arrowhead in C). Five months later, the progressive atrophy has formed a cortical CSF-filled cavity (asterisk in B). Note, how despite the similar edema size at 2 days, the chronic lesion size differs evidently (B versus D). On T2-weighted images, intracortical hematomas (black arrow in A) and white matter bleeds (black arrowhead in C) are also evident. Atrophy can be quantified by whole brain volumetry (E), or by segmenting, e.g., the enlarged ventricles and lesion cavity (F). These examples are made by ITK-SNAP on isotropic 3D high-resolution images in (G). Images were acquired at 7T with actively decoupled volume transmitter and quadrature surface receiver coils. Fast spin echo sequence (TurboRARE, effective TE = 45 ms, TR = 3400 ms, RAREfactor = 8) was used to obtain T2-weighted images, 23 slices 0.8-mm-thick with  $117 \times 117 \mu\text{m}$  in-plane resolution in 5 min. 3D images with T1/T2\* mixed contrast and  $160 \mu\text{m}^3$  isotropic resolution were obtained with a multi-echo gradient echo sequence (TR = 66 ms, 13 echoes with TE from 2.7 ms to 43 ms, flip angle  $16^\circ$ , averaged over echoes) in 11 min. Courtesy of EpiBioS4Rx project, data acquired by Riikka Immonen.

Anatomical MRI contrast is most often obtained in preclinical imaging with T2 weighting (Figure 13), even though various other MRI contrasts and sequences can be used to interrogate anatomical/structural information. Imaging parameters, preparation and acquisition schemes, and the encoding details are all crucial for the correct interpretation and identification of potential artifacts. While the scan time available and the desired spatial resolution set a framework for the volumetric information, the scan can be sensitized to various epilepsy-related brain abnormalities: T2-weighted imaging for example is sensitive to edema and decreased cell density (conditions that alter the free water content in the tissue), and can also depict hematomas (Figure 13). Quantitative T2 alterations can be used to detect hippocampal sclerosis,<sup>75,76</sup> regions affected and lesioned after traumatic brain injury,<sup>77,78</sup> after pilocarpine-induced status epilepticus,<sup>79</sup> and after febrile seizures.<sup>80</sup> T2\*-weighted imaging or susceptibility weighted imaging (applying a phase mask) will distinguish microbleeds associated with diffuse axonal and vascular injury, and thalamic calcifications typical for post-traumatic epilepsy models.<sup>81</sup> T1-weighted high-resolution 3D images are fast

to acquire and allow segmentation and quantification of brain white matter and gray matter, detection of white matter abnormalities, and elimination of the cerebrospinal fluid component by fluid attenuation techniques. In the following paragraphs and in the accompanying CRF (see Figure 14) we list some of the main methods for structural and anatomical imaging, and the key parameters to record and report.

### 3.7.2 | Measurements

Typically, T2-weighted images or a series of T2-weighted images are acquired, allowing for the calculation of echo-averaged T2-weighted image and the quantitative map. Quantitative mapping requires a set of images with varying echo time to which a signal decay curve is fitted to create a map with absolute values. Quantitative mapping allows, in principle, parameter comparison across studies and imaging centers; however, T2 time is pulse sequence and field dependent. T1-weighting/mapping can also be used; however, anatomical and lesion contrast are

## Neuroimaging Studies

Case Report Form: 07 - Volumetry.docx

CRF module: Volumetry

Date and time that this CRF was filled out:Name of person filling out CRF:Project name/Identifier:Animal ID:

| <u>CDE Name</u>   | <u>Data Collected</u>   |
|---|---|
| <b>Anatomical imaging / Volumetry</b>                           |   |
| Quantitative or weighted images                                 | <input type="checkbox"/> Quantitative map <input type="checkbox"/> Contrast-weighted <input type="checkbox"/> Unknown   |
| Sequence  | <input type="checkbox"/> Fast spin echo <input type="checkbox"/> Gradient echo <input type="checkbox"/> Spoiled GRE<br><input type="checkbox"/> Steady state GRE <input type="checkbox"/> Unknown                         |
| Specify the sequence / sequence name                            |   |
| Dimensions  | <input type="checkbox"/> 2D <input type="checkbox"/> 3D <input type="checkbox"/> Unknown  |
| Isotropic resolution  | <input type="checkbox"/> Yes <input type="checkbox"/> No <input type="checkbox"/> Unknown   |
| Resolution in mm  | _____ x _____ x _____   |
| Coverage (FOV coverage)   | <input type="checkbox"/> Whole brain <input type="checkbox"/> Cerebrum <input type="checkbox"/> Partial coverage<br><input type="checkbox"/> Unknown  |
| Contrast  | <input type="checkbox"/> T2-weighted <input type="checkbox"/> T1-weighted <input type="checkbox"/> Fluid-attenuated<br><input type="checkbox"/> T2* / SWI <input type="checkbox"/> Mixed <input type="checkbox"/> Unknown |
| <b>Imaging parameters</b>                                       |   |
| Repetition time (TR) in ms                                      |   |
| Flip angle in degrees   |   |
| Echo time (TE) / Effective echo time (TE <sub>eff</sub> ) in ms |   |
| Base echo time in ms  |   |
| Echo spacing in ms  |   |
| Number of echoes  |   |
| Otherwise: specify echo train in ms                             |   |

FIGURE 14 Volumetry case report form (see main text for details).

typically better in T2-weighted images at the high magnetic field strengths used for preclinical imaging.

A fast spin echo sequence (T2 decay) is less sensitive to susceptibility artifacts and shimming than a gradient echo sequence (T2\* decay), while gradient echo sequences are advantageous for fast 3D imaging as a small flip angle and a shorter repetition time can be used. A short TR and moderate flip angle with a short echo time yield T1-weighted contrast, and the longer the TE the more T2\*-weighting is added. In steady-state gradient echo sequences, the “dynamic equilibrium,” i.e., the steady state, is achieved after a set of dummy scans ( $>5 \cdot T1$ ) and a higher signal-to-noise ratio per time period can be achieved typically with mixed T1 and T2 contrast. In balanced steady-state free precession (bSSFP) acquisitions when all gradients are balanced, contrast is more T2-weighted. Phase cycling can be used to mitigate the banding artifacts that are typical of this acquisition scheme. Inflowing blood appears bright.

Multi-slice (2D) or 3D data with isotropic or anisotropic voxels, and the exact spatial resolution are all critical features. The higher the resolution, the more averaging is needed for a sufficient signal-to-noise ratio, at a cost in scan time. Partial k-space sampling and phase-encoding direction are to be specified, but placing the readout along the long axis of the brain can be used to reduce scan time by decreasing the number of phase-encoding steps required. Typical resolution in rats is in-plane from  $80 \times 80 \mu\text{m}^2$  to  $200 \times 200 \mu\text{m}^2$ , when the slice thickness is 0.5–0.8 mm. Isotropic resolution is preferable, especially if contemporary analysis pipelines (including co-registration) are used. Typical isotropic resolution for the rat brain is  $150\text{--}300 \mu\text{m}^3$ .

Anatomical images can have T2-weighted, T1-weighted, T2\*-weighted or mixed contrast. Typically, T2-weighted gives the best white matter/gray matter contrast and best highlights the lesion in high  $B_0$  strength. If fluid attenuation is used it has to be stated for the correct

|  |   |
|--|---|
| Inversion time (inversion recovery T1) in ms |   |
| Specify array                                |   |
| <b>k-space coverage / encoding</b>           |   |
| Partially parallel imaging acceleration      | <input type="checkbox"/> Yes <input type="checkbox"/> No <input type="checkbox"/> Unknown   |
| Partial-FT acceleration                      | <input type="checkbox"/> Yes <input type="checkbox"/> No <input type="checkbox"/> Unknown   |
| Zero-filled acceleration                     | <input type="checkbox"/> Yes <input type="checkbox"/> No <input type="checkbox"/> Unknown   |
| Other acceleration method                    |   |
| Read direction                               | <input type="checkbox"/> S-I (superior-inferior) <input type="checkbox"/> L-R (left-right)<br><input type="checkbox"/> H-F (head-feet) <input type="checkbox"/> Unknown |
| <b>Analysis</b>                              |   |
| Image reconstruction and analysis pipeline   |   |

**Parameters**

|  |  |  |  |  |  |  |
|--|--|--|--|--|--|--|
| Imaging date and time                  |  |  |  |  |  |  |
| Time Point after initial insult (days) |  |  |  |  |  |  |

**Instructions:** Please check boxes where applicable. If none of the predetermined options is appropriate use the default space to specify your answer. This form is to be filled in for one individual animal.

**FIGURE 14** (Continued)

interpretation of images. Susceptibility-weighted images and quantitative susceptibility maps can be generated by exploiting the phase information in T2\*-weighted images. The signal intensity and image contrast depend on the repetition time (TR), flip angle, effective echo time (TE) or the echo train, and the inversion time in inversion recovery T1-weighted imaging. In gradient echo sequences, the flip angle for the highest signal intensity is given by the Ernst angle, which can be calculated for the selected TR if tissue T1 is known.

### 3.7.3 | Equipment

Anatomical imaging does not set any extra requirements for equipment beyond that mentioned in the Technical information section.

### 3.7.4 | Procedure

No preparation of the animal is needed. Animals are scanned under inhalation anesthesia (typically isoflurane), head-fixed by ear bars and a teeth bar to eliminate movement artifacts. Breathing rate and temperature should be monitored to maintain the anesthesia level, animal stability, and temperature.

### 3.7.5 | Analysis and interpretation

A wide variety of methods and toolboxes are available for volumetric analyses. In the injured rodent brain, they often require study-specific optimization, user interference, and manual refinement. The first preprocessing step of the analysis pipeline is often the skull stripping/brain extraction. The next steps, co-registration and/or segmentation, strongly rely on sufficient tissue contrast and signal-to-noise ratio. Brain atlases are available for different rat/ mouse strains, and different MRI contrasts. Atrophy can be assessed via ROI analysis, voxel-based morphometry, tensor-based morphometry, and deformation matrices, shape analyses, or surface analyses. Key toolboxes include FSL,<sup>82,83</sup> ANTs,<sup>84</sup> ITK-SNAP,<sup>85</sup> and SPM (<https://www.fil.ion.ucl.ac.uk/spm/>). See, e.g., Feo and Giove<sup>86</sup> for a critical review regarding rodent applications, and software listing with references.

## 3.8 | Manganese contrast-enhanced magnetic resonance imaging

CRF File name: 08 CRF module - Manganese contrast-enhanced MRI.docx

CDE File name: 08 CDE chart - Manganese contrast-enhanced imaging.xlsx ([Supporting information](#))

### 3.8.1 | Rationale

Manganese-enhanced MRI (MEMRI) can be utilized in preclinical epilepsy research to visualize anatomical details, brain activity, or circuitry reorganization such as axonal sprouting.<sup>87–90</sup> The paramagnetic manganese ion,  $Mn^{2+}$ , is an MRI contrast agent and a  $Ca^{2+}$  analog. Sharing the same transport systems as  $Ca^{2+}$ ,  $Mn^{2+}$  is taken up during neuronal depolarization/action potential. As such, manganese can be transported along axons both anterogradely and retrogradely, and across synapses, highlighting thereby the entire fiber tract, and pathological

alterations therein (Figure 15). Structural MEMRI allows also discerning cortical laminar architecture.<sup>91</sup>

Manganese uptake is neuronal activity-dependent; however, it is often limited by low BBB penetration, and experimental protocols/methodology that utilize different types of stimulation schemes are called activity-induced manganese-dependent MRI (AIM-MRI),<sup>92–94</sup> or dynamic AIM (DAIM) when the dynamics of Manganese accumulation is captured.<sup>92</sup> In this section, as well as in the accompanying CRF (see also Figure 16), we describe the details for structural MEMRI, while for dynamic activity-dependent imaging the reader is referred to the literature.<sup>92,93,95</sup>

### Manganese enhanced MRI of mossy fiber sprouting

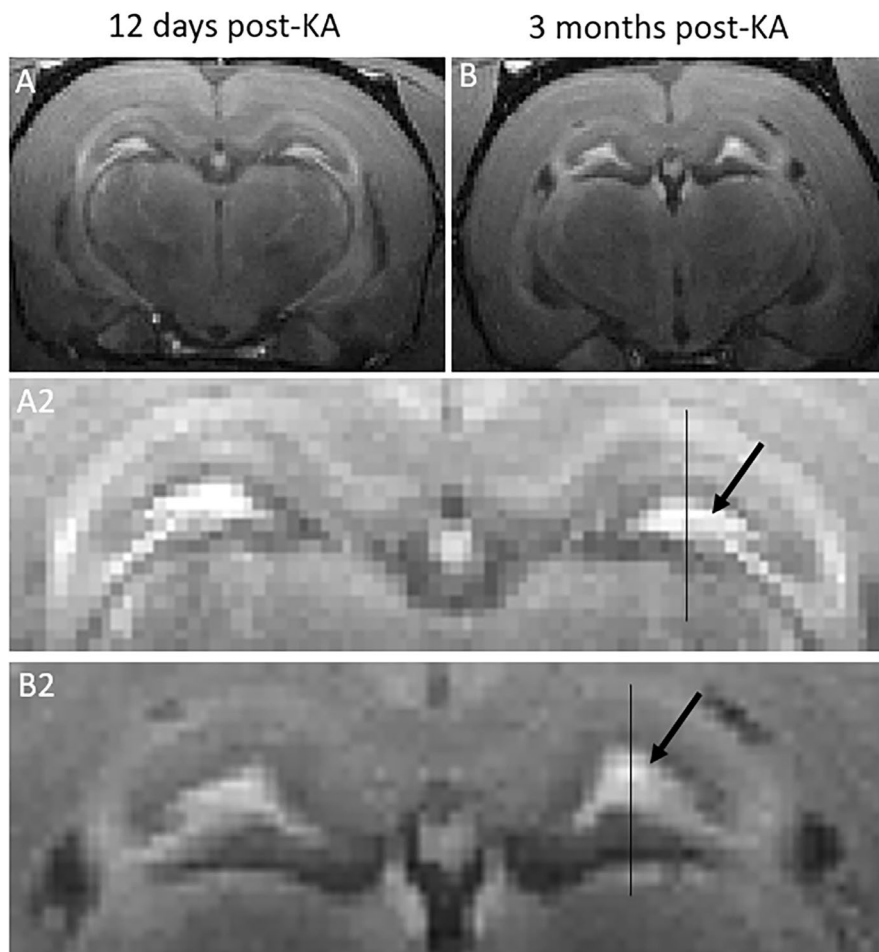


**FIGURE 15** Manganese-enhanced MRI (MEMRI) highlights the perforant pathway and mossy fiber sprouting in the dentate gyrus, allowing longitudinal studies of hippocampal axonal plasticity during epileptogenesis. Panel shows T1-weighted images 24 h after intraperitoneal  $MnCl_2$  administration 12 days (A, A2) and 3 months (B, B2) after kainic acid (KA)-induced status epilepticus. The area of manganese-enhanced signal in the dentate gyrus (black arrows) increases upon axonal sprouting. Intensity profiles across hippocampi (lines) allow assessing the thickness of different hippocampal layers. Histological assessment has shown manganese to accumulate into mossy fibers but also co-located astrogliosis may contribute to the contrast.<sup>87</sup> T1-weighted 3D images were acquired at 4.7T with quadrature surface RF coil using gradient echo sequence with an adiabatic 70-degree BIR-4 excitation pulse to reduce the influence of B1 inhomogeneity (TR = 120 ms, TE = 2.7 ms, volume of  $2.5 \times 2.5 \times 3.5 \text{ cm}^3$  was covered with  $192 \times 64 \times 256$  points). Data acquired by Riikka Immonen.

**Neuroimaging Studies****Case Report Form: 08 CRF- Manganese contrast-enhanced imaging.docx****CRF module: Manganese contrast-enhanced imaging**

Date and time that this CRF was filled out:

Name of person filling out CRF:

Project name/Identifier:

Animal ID:

| <u>CDE Name</u>   | <u>Data Collected</u>   |
|---|---|
| <b>Manganese (II) chloride (MnCl<sub>2</sub>) administration</b>                            |   |
| Route of administration   | <input type="checkbox"/> Intraperitoneal <input type="checkbox"/> Intravenous <input type="checkbox"/> Intracerebral <input type="checkbox"/><br>Subcutaneous <input type="checkbox"/> Unknown <input type="checkbox"/> Other |
| If other, please specify  |   |
| Dose mg/kg  |   |
| Concentration in mM   |   |
| Buffer  |   |
| pH  |   |
| Volume administered ml  |   |
| Time of MnCl <sub>2</sub> administration pre-scan (time prior to scan) in hours and minutes |   |
| Number of seizures between MnCl <sub>2</sub> injection and start of imaging session         |   |
| <b>MEMRI imaging</b>  |   |
| Baseline scan without manganese   | <input type="checkbox"/> Yes <input type="checkbox"/> No <input type="checkbox"/> Unknown   |
| Imaging time points after MnCl <sub>2</sub> administration                                  | _____   |
| Quantitative or weighted images   | <input type="checkbox"/> Quantitative map<br><input type="checkbox"/> Contrast-weighted<br><input type="checkbox"/> Unknown   |
| Sequence  | <input type="checkbox"/> Fast spin echo <input type="checkbox"/> Gradient echo <input type="checkbox"/> Spoiled GRE   |

**FIGURE 16** Manganese contrast-enhanced magnetic resonance imaging case report form (see main text for details)

### 3.8.2 | Measurements

A baseline scan prior to any MnCl<sub>2</sub> contrast agent can be acquired, but it needs to be in a separate scanning session in the case of systemic administration, for it takes manganese several hours to reach the brain structures of interest. For intracerebral injection, the animal needs to be removed from the scanner for MnCl<sub>2</sub> delivery. The pattern of MEMRI contrast in the brain depends on the time point for imaging from the MnCl<sub>2</sub> administration (see below, the procedure paragraph).

Manganese shortens both the longitudinal and the transverse relaxation time, creating a positive contrast enhancement in T1-weighted and negative in T2-weighted images. Typically for MEMRI, the T1-weighted imaging is utilized and it shows the white matter tracts and other sites of manganese accumulation with high signal intensity. Quantitative T1 mapping allows for indirect assessment of the manganese concentrations, that is, the amount of the accumulated manganese in the target structures. T1

mapping is done by inversion recovery sequence or saturation recovery. Regarding the sequence and spatial resolution, the same principles apply to the anatomical/volumetry imaging (see CRF7).

### 3.8.3 | Equipment

No extra requirement for hardware beyond that described in the Technical details section is needed. However, MEMRI benefits from a high field magnet system, since the contrast enhancement is magnetic field strength-dependent and a high spatial resolution for anatomical details is desired.

### 3.8.4 | Procedure

For structural MEMRI, the contrast agent is often given several hours before the scan, even 24 h earlier. The timing depends on the route of administration and whether

|   |   |
|---|---|
|   | <input type="checkbox"/> Steady state GRE <input type="checkbox"/> Unknown  |
| Dimensions                              | <input type="checkbox"/> 2D <input type="checkbox"/> 3D <input type="checkbox"/> Unknown  |
| Isotropic resolution                    | <input type="checkbox"/> Yes <input type="checkbox"/> No <input type="checkbox"/> Unknown   |
| Resolution in mm                        | _____ x _____ x _____   |
| Coverage (FOV coverage)                 | <input type="checkbox"/> Whole brain <input type="checkbox"/> Cerebrum <input type="checkbox"/> Partial coverage<br><input type="checkbox"/> Unknown  |
| Contrast                                | <input type="checkbox"/> T2-weighted <input type="checkbox"/> T1-weighted <input type="checkbox"/> Mixed <input type="checkbox"/> Inversion<br>recovery T1 <input type="checkbox"/> Fluid-attenuated <input type="checkbox"/> Unknown |
| Echo time (TE) in ms                    |   |
| Repetition time (TR) in ms              |   |
| Flip angle in degrees                   |   |
| Inversion time (TI) in ms               |   |
| Specify array                           |   |
| <b>k-space coverage / encoding</b>      |   |
| Partially parallel imaging acceleration | <input type="checkbox"/> Yes <input type="checkbox"/> No <input type="checkbox"/> Unknown   |
| Partial-FT acceleration                 | <input type="checkbox"/> Yes <input type="checkbox"/> No <input type="checkbox"/> Unknown   |
| Zero-filled acceleration                | <input type="checkbox"/> Yes <input type="checkbox"/> No <input type="checkbox"/> Unknown   |
| Other acceleration method               |   |
| Read direction                          | <input type="checkbox"/> S-I (superior-inferior) <input type="checkbox"/> L-R (left-right)<br><input type="checkbox"/> H-F (head-feet) <input type="checkbox"/> Unknown   |
| <b>Analysis</b>                         |   |
| Analysis pipeline                       |   |

**Parameters**

|  |  |  |  |  |  |  |
|--|--|--|--|--|--|--|
| Imaging date and time                  |  |  |  |  |  |  |
| Time Point after initial insult (days) |  |  |  |  |  |  |

**Instructions:** Please check boxes where applicable. If none of the predetermined options is appropriate use the default space to specify your answer. This form is to be filled in for one individual animal.

FIGURE 16 (Continued)

any stimulation paradigm is applied during manganese accumulation into the brain. The route of administration, timing relative to the scan, the compound, dose, and pH are to be reported as CDEs. Conditions (stimulation or seizure activity) during the manganese accumulation should also be noted. Anesthesia during the scan does not play a major role in the case of structural MEMRI where Mn<sup>2+</sup> accumulation occurs prior to the scan itself.

### 3.8.5 | Systemic administration of manganese

A manganese chloride (MnCl<sub>2</sub>) buffer is usually bicine and the pH needs to be adjusted to the physiological range. MnCl<sub>2</sub> can be administered systemically via intraperitoneal or subcutaneous injection. For dosage and methodological details, see.<sup>91,96,97</sup> Typical systemic MnCl<sub>2</sub> doses range from 30 to 175 mg/kg. For systemic administration, it takes 5-8 h for the contrast agent to pass across the chorooid plexus and reach the ventricular system (ventricles

are highlighted after 7 h, while parenchyma remains unaffected), and then, the final accumulation pattern highlighting the axonal tracts/fiber bundles/pathways is found 20-24 h after the injection. The MEMRI contrast is sustained until approximately 48 h and decays thereafter. The complete clearance of manganese has been reported to take 10 days.<sup>98</sup> Intravenous MnCl<sub>2</sub> injection may induce heart issues (increased heart rate, cardiac arrest) and has to be tested in each animal model. For structural MEMRI, the dose can be fractionated, e.g., dose divided into three injections with fewer side-effects.<sup>99</sup> Subcutaneous injections may evoke skin irritation.

### Intracerebral administration of manganese

MnCl<sub>2</sub> injections directly into the brain allow targeting of a certain pathway, e.g., direct injections into the thalamus have been utilized to assess thalamocortical projections,<sup>91</sup> or injections into the cortex, the cortico-thalamic,<sup>89</sup> or interhemispheric cortico-cortical connectivity.<sup>90</sup>

A drawback of manganese is its cellular toxicity and therefore manganese contrast agents are not used for brain research in the clinic. In the study design, the potential adverse effects of manganese should be accounted for, e.g., showing in a control group the absence of any effect by contrast agent alone.

In epilepsy studies, manganese accumulation will depend on any seizure activity during the contrast agent absorption period. Hence, the seizure activity should be monitored after the manganese administration until the scan. Animals with seizures can then be analyzed as a separate group, or the seizure activity should be taken into account as a confounding factor.

### 3.8.6 | Analysis and interpretation

In structural MEMRI studies the snapshot situation, e.g., 24h postsystemic MnCl<sub>2</sub> is captured instead of following the dynamics of contrast agent accumulation.

Analysis approaches are (a) characterization of the properties of the white matter tracts enhanced: discontinuity, thickening, axonal sprouting, (b) relative signal enhancement in an ROI, or (c) quantitative T1 alterations.

## 3.9 | Functional magnetic resonance imaging

CRF File name: 09 CRF module - Functional MRI.docx

CDE File name: 09 CDE chart - Functional MRI.xlsx  
([Supporting information](#))

### 3.9.1 | Rationale

fMRI detects brain activation indirectly as neuronal activity is closely linked to the vascular response (so-called neurovascular coupling). As a result, cerebral blood volume (CBV), cerebral blood flow (CBF), and blood oxygenation increase during brain activation, all of which can be detected by MRI. Most often blood oxygenation level-dependent (BOLD) contrast is used, which is based on different magnetic susceptibilities of oxygenated and deoxygenated hemoglobin in blood, leading to signal intensity changes in T2(\*)-weighted images. In addition, intravascular iron-based T2(\*) contrast agents can be utilized to sensitize T2(\*)-weighted imaging to CBV changes, which provides better contrast to noise than BOLD. However, this requires i.v. contrast agent injections and normalization for contrast agent washout, and is therefore more complicated in practice, especially in longitudinal study designs.

Typically, fMRI is used to measure changes in brain activity over time. The change can be due to external

stimulations, epileptiform activity or seizures, brain state changes, or naturally occurring resting-state fluctuations in brain activity, which are correlated with functionally connected brain areas. In the context of epilepsy, epilepsy-related brain activity is most often measured simultaneously with fMRI and electrical recordings, or the resting state fMRI signal is recorded to analyze changes in large-scale functional connectivity during epileptogenesis/epilepsy. In this section, as well as in the accompanying CRF (see also [Figure 17](#)), we describe the details for fMRI.

### 3.9.2 | Measurements

Before the actual fMRI part, high-resolution anatomical imaging with a T2-weighted (TE~T2, TR = 1.5-3s) fast spin-echo sequence is performed to provide an anatomical reference to which lower-resolution functional images are co-registered.

fMRI requires the mapping of temporal changes in signal intensity with high temporal resolution. In practice, this is achieved by single-shot EPI. Prior to EPI scanning, automated 3D field map-based shimming should be performed and linewidth documented. Gradient echo EPI provides better contrast-to-noise than SE-EPI and better temporal resolution can be used by combining less than a 90-degree flip angle with shorter TR; however, spin-echo EPI can also be used especially in cases where magnetic field homogeneity is compromised by implanted electrodes or invasive surgery. The echo time should be in the order of T2 for SE-EPI and T2\* for GE-EPI, and TR of 1-2s should be used. Isotropic resolution is preferable, typical resolution of 0.3-0.4 mm<sup>3</sup>. High readout bandwidth (~200 kHz, typically limited by gradient performance and heating) should be used to limit the length of echo train and to reduce field inhomogeneity-related artifacts. Fat suppression is typically used and outer-volume suppression can also be used for the smaller field of views.

New fMRI pulse sequences with zero echo time and very high bandwidth in three directions are becoming available for fMRI with an extremely high tolerance for magnetic susceptibility artifacts and small induction of EEG artifacts, features that make them optimal for fMRI studies with animals with implanted electrodes.<sup>100</sup>

### 3.9.3 | Equipment

fMRI benefits from a high magnetic field, which increases BOLD contrast and the signal-to-noise ratio. In experiments where magnetic susceptibility difference related to field inhomogeneity is an issue (e.g., implanted electrodes), the high magnetic field can, however, be non-advantageous, as the magnetic susceptibility scales with

the magnetic field. A well-performing gradient system is an absolute requirement because EPI with high read bandwidth has to be used to limit susceptibility-related artifacts. A standard transmit/volume coil-quadrature/multichannel surface receiver coil -pair can be used in most cases. In animals with head implants (e.g., chronically implanted EEG electrodes) a linear single loop surface coil (either receive only or transceiver) can be used around the implant or implanted on the skull.<sup>101</sup>

In addition to standard physiological monitoring (breathing rate, temperature), blood oxygenation and CO<sub>2</sub> should also be monitored. The recommended way is to use a blood gas analyzer and measure the blood gases from arterial blood samples. In longitudinal studies, repeated cannulation for blood sampling can be a problem and noninvasive measurements using a pulse oximeter

and a capnography device can be used. These are clearly less reliable approaches than blood gas analysis in small animals, and this kind of noninvasive setup should be always validated against blood gas analysis. Either a volume or pressure-controlled ventilator for mechanical ventilation is often needed to maintain normal blood gases under anesthesia.

### 3.9.4 | Procedure

Animals are typically anesthetized for fMRI even though awake fMRI approaches exist.<sup>21</sup> The type of anesthesia influences the results and there is currently no agreement in the field about the best anesthesia.<sup>14,102,103</sup> For longitudinal studies, medetomidine or the combination

#### Neuroimaging Studies

Case Report Form: 09 CRF - Functional MRI.docx

CRF module: Functional MRI

Date and time that this CRF was filled out:

Name of person filling out CRF:

Project name/Identifier:

Animal ID:

| CDE Name                               | Data Collected   |
|--|--|
| <b>Resting state fMRI</b>              |  |
| Imaging sequence                       | <input type="checkbox"/> Gradient echo - Echo Planar Imaging<br><input type="checkbox"/> Spin-Echo - Echo Planar Imaging<br><input type="checkbox"/> Unknown<br><input type="checkbox"/> Other |
| If other, please specify               |  |
| Contrast agent (CBV fMRI)              | <input type="checkbox"/> Yes <input type="checkbox"/> No <input type="checkbox"/> Unknown  |
| Contrast agent Name/Type               |  |
| Contrast agent dose in mg/kg           |  |
| <b>fMRI imaging parameters</b>         |  |
| Dimension                              | <input type="checkbox"/> 2D <input type="checkbox"/> 3D <input type="checkbox"/> Unknown   |
| Isotropic resolution                   | <input type="checkbox"/> Yes <input type="checkbox"/> No <input type="checkbox"/> Unknown  |
| Number of slices (1 if 3D)             |  |
| Slice thickness / slab thickness in mm |  |
| FOV coverage                           | <input type="checkbox"/> Whole brain <input type="checkbox"/> Cerebrum <input type="checkbox"/> Partial coverage<br><input type="checkbox"/> Unknown   |
| FOV in mm                              | _____ x _____ x _____  |
| Matrix / number of points              | _____ x _____ x _____  |
| Repetition time (TR) in ms             |  |
| Flip angle in degrees                  |  |

**FIGURE 17** Functional parcellation of a normal rat brain obtained by independent component analysis with 45 components (A). Functional connectivity matrices from correlation analysis between atlas-based brain areas from 20 rats before (B) and 10 days after traumatic brain injury (C). Data acquired by Lenka Dvorakova and Olli Gröhn at the University of Eastern Finland. <sub>c</sub>, contralateral to injury; <sub>i</sub>, ipsilateral to injury; AU, auditory cortex; CA, Hippocampus; cG, cingula cortex; CPu, caudate putamen; HTh, Hypothalamus; M1M2, motor cortex; mPFC, medial prefrontal cortex; MTh, medial thalamus; PtA, parietal cortex; RSc, retrosplenial cortex; S1S2, somatosensory cortex; V1V2, visual cortex; VLTh, ventrolateral thalamus.

|  |   |
|--|---|
| Echo time (TE) / Effective echo time (TEeff) in ms |   |
| base echo time in ms                               |   |
| echo spacing in ms                                 |   |
| Number of echoes                                   |   |
| otherwise: specify echo train in ms                |   |
| Read Bandwidth in kHz                              |   |
| Fat suppression                                    | <input type="checkbox"/> Yes <input type="checkbox"/> No <input type="checkbox"/> Unknown   |
| Outer volume suppression                           | <input type="checkbox"/> Yes <input type="checkbox"/> No <input type="checkbox"/> Unknown   |
| Number of dummy scans                              |   |
| Number of images                                   |   |
| <b>k-space coverage / encoding</b>                 |   |
| Partially parallel imaging acceleration            | <input type="checkbox"/> Yes <input type="checkbox"/> No <input type="checkbox"/> Unknown   |
| Partial-FT acceleration                            | <input type="checkbox"/> Yes <input type="checkbox"/> No <input type="checkbox"/> Unknown   |
| Zero-filled acceleration                           | <input type="checkbox"/> Yes <input type="checkbox"/> No <input type="checkbox"/> Unknown   |
| Read direction                                     | <input type="checkbox"/> S-I (superior-inferior) <input type="checkbox"/> L-R (left-right)<br><input type="checkbox"/> H-F (head-feet) <input type="checkbox"/> Unknown         |
| Phase1 direction                                   | <input type="checkbox"/> S-I (superior-inferior) <input type="checkbox"/> L-R (left-right) <input type="checkbox"/> H-F (head-feet) <input type="checkbox"/> Unknown            |
| <b>fMRI analysis</b>                               |   |
| <b>Pre-processing</b>                              |   |
| Slice-timing correction                            | <input type="checkbox"/> Yes <input type="checkbox"/> No <input type="checkbox"/> Unknown   |
| Motion correction                                  | <input type="checkbox"/> Yes <input type="checkbox"/> No <input type="checkbox"/> Unknown   |
| Co-registration to a template brain                | <input type="checkbox"/> Yes <input type="checkbox"/> No <input type="checkbox"/> Unknown   |
| Smoothing with a Gaussian, FWHM sigma in mm        |   |
| <b>Analysis</b>                                    |   |
| Method   | <input type="checkbox"/> ROI-based resting state maps<br><input type="checkbox"/> Group resting-state ICA<br><input type="checkbox"/> Unknown<br><input type="checkbox"/> Other |
| If other, please specify                           |   |
| Functional connectivity analysis pipeline          |   |

**Parameters**

|  |  |  |  |  |  |  |
|--|--|--|--|--|--|--|
| Imaging date and time                  |  |  |  |  |  |  |
| Time Point after initial insult (days) |  |  |  |  |  |  |

**Instructions:** Please check boxes where applicable. If none of the predetermined options is appropriate use the default space to specify your answer. This form is to be filled in for one individual animal.

FIGURE 17 (Continued)

of medetomidine and isoflurane are good choices, while alpha-chloralose and urethane can be used in terminal studies (see Physiology section for details). Animals often undergo surgery before fMRI scanning, for example, cannulation allowing arterial blood sampling and/or infusion of a sedative/anesthetic when needed. Any immediate prescanning surgical procedures should be conducted under general anesthesia, typically isoflurane, after which the animal is transferred to the animal

holder. With most anesthetics, mechanical ventilation *per os* (longitudinal studies) or via the trachea (terminal studies) is required. After preoperation, the animal is switched to a different sedation/anesthesia for fMRI. Time spend in isoflurane anesthesia and time between cessation of isoflurane anesthesia and the beginning of fMRI should be kept constant and documented. The animal's head is fixed with ear bars and a teeth bar and probes for physiological monitoring are attached to the

animal (this can still be done during deeper anesthesia). Physiological monitoring is performed continuously and values recorded. Blood gases should be analyzed minimum once during the experiment, preferably at the beginning and at the end of the fMRI scanning.

### 3.9.5 | Analysis and interpretation

The purpose of fMRI analysis is to identify small signal changes, on the order of a few percent of the baseline signal, or to investigate temporal correlations of signal fluctuations. A myriad of different fMRI analysis approaches and software packages, such as Statistical Parametrical Mapping (SPM, <https://www.fil.ion.ucl.ac.uk/spm/>), the FMRIBSoftware Library (FSL, <https://fsl.fmrib.ox.ac.uk/fsl/fslwiki/>) and Analysis of Functional NeuroImages (AFNI, <https://afni.nimh.nih.gov/>), exist. Typically, an fMRI analysis pipeline consists of the following steps: slice timing correction, motion correction, co-registration to a common template for group-level analysis, and spatial smoothing. When the duration of the activation is known from the stimulation paradigm or simultaneous EEG measurements, a general linear model can be used to determine activated voxels. For that, the assumed brain activation time course is convolved with a hemodynamic response function (HRF) to obtain the presumed fMRI

time course. It should be noted that many fMRI software packages use human HRFs as a default, and for the rodent fMRI analysis that should be changed to shorter HRF corresponding better to rodent HRF.<sup>104</sup> In the actual analysis, correlations of presumed signal time courses and measured signal time courses are analyzed voxel-wise. As fMRI volumes consist of thousands of voxels, multiple comparison bias becomes a major issue for statistical analysis. There are multiple demonstrations of false-positive findings<sup>105</sup> if correction is not done, while more stringent multiple comparison correction approaches result in false negatives and loss of true activation. Currently, the family-wise error (FWE) correction, Bonferroni correction, and false discovery rate (FDR) correction are widely used.

For the analysis of functional connectivity, similar preprocessing steps are performed followed by seed-based or predetermined regions of interest (ROI)-based correlation analysis. Here, clear hypotheses, whenever possible, should be used to reduce the number of multiple comparisons. Graph theory-based approaches (see<sup>106</sup> for review) are nowadays gaining popularity, as they allow for the analysis of data at the network level. Also, data-driven approaches such as independent component analysis (ICA) can be used (Figure 18). These are especially useful for the initial screening of new data.

For all interpretations, it is important to realize that fMRI measures brain activity indirectly through

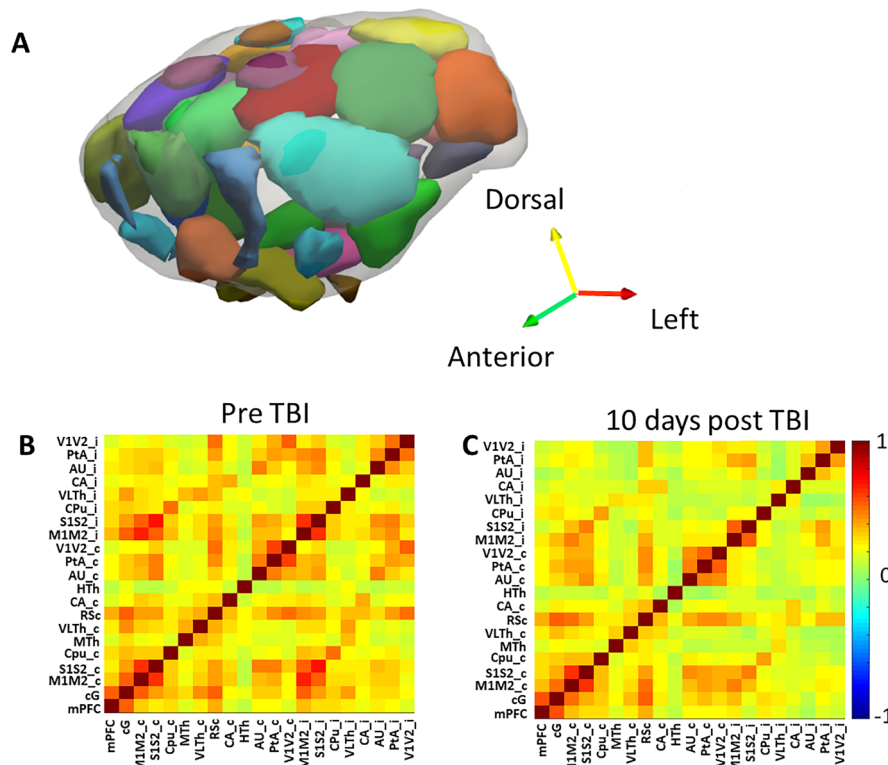


FIGURE 18 fMRI case report form (see main text for details)

neurovascular coupling, and in damaged brain areas, this neurovascular coupling may be disturbed.

### 3.10 | <sup>1</sup>H Magnetic resonance spectroscopy

CRF File name: 10 CRF module - 1H Magnetic resonance spectroscopy.docx

CDE File name: 10 CDE chart - 1H Magnetic resonance spectroscopy.xlsx ([Supporting information](#))

#### 3.10.1 | Rationale

Proton magnetic resonance spectroscopy (1H-MRS) enables the noninvasive detection and quantification of brain metabolites including the excitatory neurotransmitter glutamate as well as GABA and glutamine. As such, 1H-MRS is a potentially powerful tool for epilepsy research enabling not only the investigation of metabolic mechanisms underlying epilepsy<sup>107</sup> and/or may provide useful biomarkers to predict seizures, for example, markers of

gliosis and astrocyte activation,<sup>108–110</sup> or together with more general markers of cell death.<sup>111</sup> The volume of interest from which 1H-MRS spectra are acquired ([Figure 19](#)) can be positioned anywhere in the brain parenchyma and therefore offers distinct advantages over serum and CSF-based biomarkers. Furthermore, MRS has been shown to detect metabolite changes in normal-appearing tissue and therefore may be a powerful biomarker for the early detection of pathophysiology. In this section, as well as in the accompanying CRF (see also [Figure 20](#)), we describe the details for MRS.

#### 3.10.2 | Measurements

Point-RESolved Spectroscopy (PRESS) with outer-volume suppression is the default acquisition scheme for single voxel-based data acquisition on the majority of preclinical scanners. Water suppression is a requirement and typical suppression schemes are CHES and VAPOR. The typical square or rectangular volume of interest (VOI) should be carefully chosen using a detailed anatomical scan for correct positioning. Placement of the VOI in brain tissue to

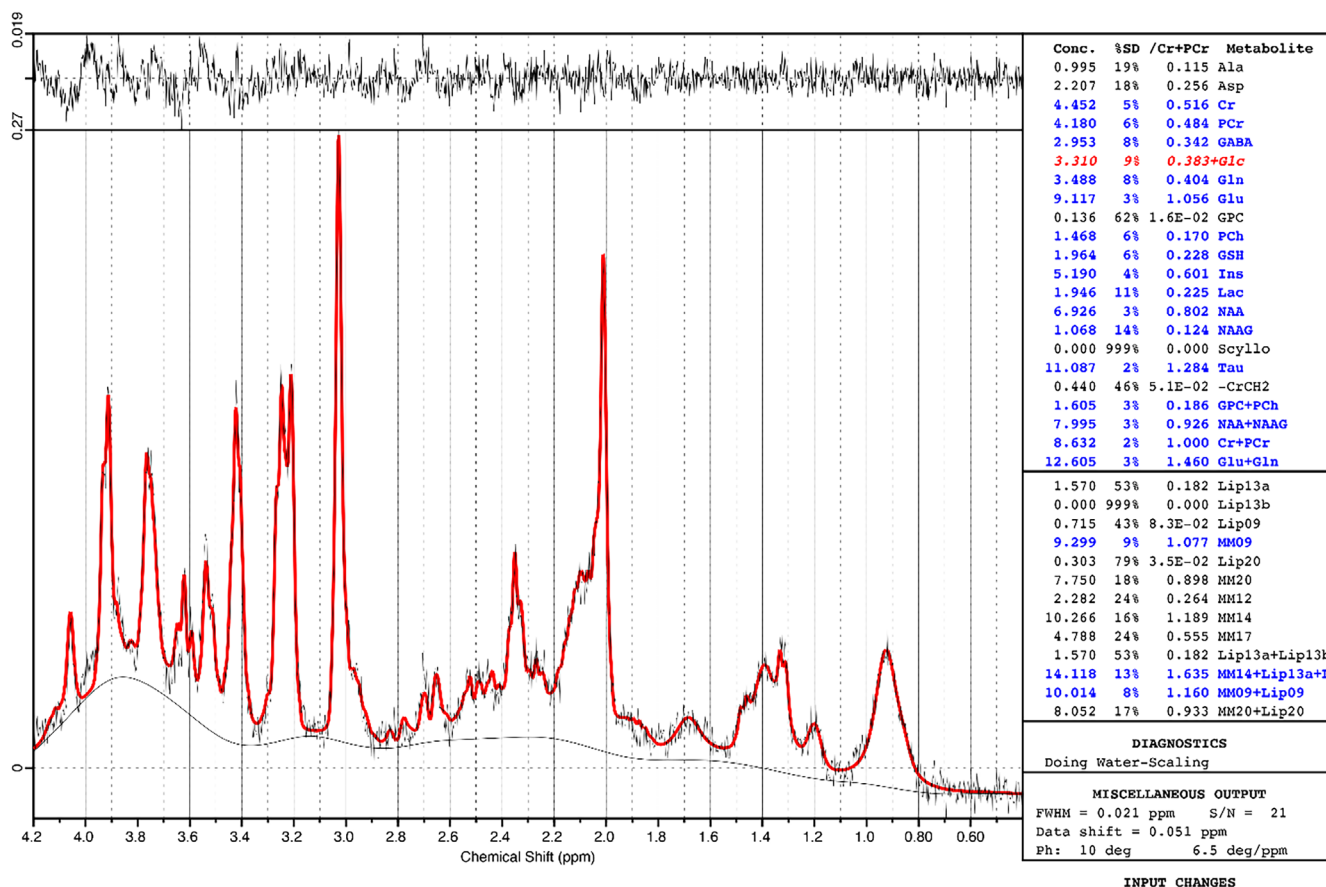


**FIGURE 19** Example spectra acquired from the mouse hippocampus. A cryogenically cooled 4-channel surface coil and PRESS sequence were used to acquire 384 averages in 16 min. The volume of interest had dimensions of  $2 \times 1 \times 1.5 \text{ mm}^3$ . The spectra were processed with LCModel using an additional acquisition without water suppression. Data acquired by David Wright.

## Neuroimaging Studies

Case Report Form: 10 CRF - 1H Magnetic resonance spectroscopy.docx

CRF module: 1H Magnetic resonance spectroscopy

Date and time that this CRF was filled out:Name of person filling out CRF:Project name/Identifier:Animal ID:

| <u>CDE Name</u>                                      | <u>Data Collected</u>  |
|--|--|
| <b>1H - Magnetic resonance spectroscopy (1H-MRS)</b> |  |
| MRS Localization method                              | <input type="checkbox"/> PRESS <input type="checkbox"/> STEAM <input type="checkbox"/> semi-LASER <input type="checkbox"/> Unknown<br><input type="checkbox"/> Other |
| If other, please specify                             |  |
| Voxel #1   |  |
| Voxel-1 location target structure                    |  |
| Voxel-1 location                                     | <input type="checkbox"/> Unilateral<br><input type="checkbox"/> Bilateral<br><input type="checkbox"/> Unknown  |
| Voxel-1 size in mm                                   | _____ x _____ x _____  |
| Voxel #2   |  |
| Voxel-2 location target structure                    | _____<br>_____   |
| Voxel-2 location                                     | <input type="checkbox"/> Unilateral<br><input type="checkbox"/> Bilateral<br><input type="checkbox"/> Unknown  |
| Voxel-2 size   | _____ x _____ x _____ mm   |
| <i>(repeat for all voxels)</i>                       | <i>(repeat for all voxels)</i>   |
| Repetition time (TR) in milliseconds                 |  |
| Echo time (TE) in milliseconds                       |  |

FIGURE 20 MRS case report form (see main text for details)

maximize the volume filled with uniform brain structure and minimize the inclusion of areas with CSF or edema will improve the shimming and thus the signal quality. The size of the VOI will not only affect interpretation of the data by the degree of normal-appearing tissue or multiple brain regions included within the VOI, but it will directly affect the length of the scan. Since the signal is proportional to the square root of the acquisition time, larger VOIs will produce more signal/scan at the expense of inclusion of multiple tissue types, and thus require less time scanning to reach a target signal-to-noise.

### 3.10.3 | Equipment

There is no substitute for increased field strength when trying to separate metabolites of interest. The long recovery times necessitated for 1H-MRS place less demand on gradient systems, however, as with other imaging

modalities, small voxel sizes benefit from the increased sensitivity afforded by anatomically shaped surface coils or small, single-turn surface coils. Short, high bandwidth RF pulses should be used to minimize chemical shift displacement, which requires RF amplifiers and transmits RF coils that can produce high B1.

### 3.10.4 | Procedure

Sedation medication is pertinent to the acquisition, especially for GABA levels, which reduce by up to 38% under isoflurane.<sup>112</sup> 1H-MRS is greatly affected by field inhomogeneity and therefore care should be taken in positioning the sample at the iso-center of the magnet and optimizing shims for the voxel of interest. Furthermore, in models of post-traumatic epilepsy, the focal injury site can also be a source of significant susceptibility changes and should be considered when positioning the voxel and designing the

|                                |   |
|--------------------------------|---|
| Bandwidth in kHz               |   |
| Number of points               |   |
| Number of averages             |   |
| OVS/ Saturation bands          | <input type="checkbox"/> Yes <input type="checkbox"/> No <input type="checkbox"/> Unknown   |
| Water suppression method       | <input type="checkbox"/> VAPOR <input type="checkbox"/> CHESS <input type="checkbox"/> Unknown <input type="checkbox"/> Other               |
| If other, please specify       |   |
| Water reference scan           | <input type="checkbox"/> Yes <input type="checkbox"/> No <input type="checkbox"/> Unknown   |
| Shimming method                | <input type="checkbox"/> FASTMAP; <input type="checkbox"/> MAPSHIM; <input type="checkbox"/> Unknown <input type="checkbox"/> Other         |
| If other, please specify       |   |
| Obtained water linewidth in Hz |   |
| <b>Analysis</b>                |   |
| Spectral analysis method       | <input type="checkbox"/> LC model <input type="checkbox"/> JMRUI, Amares <input type="checkbox"/> Unknown<br><input type="checkbox"/> Other |
| If other, please specify       |   |

**Parameters**

|  |  |  |  |  |  |  |
|--|--|--|--|--|--|--|
| Imaging date and time                  |  |  |  |  |  |  |
| Time Point after initial insult (days) |  |  |  |  |  |  |

**Instructions:** Please check boxes where applicable. If none of the predetermined options is appropriate use the default space to specify your answer. This form is to be filled in for one individual animal.

**FIGURE 20** (Continued)

study. Shimming should be conducted ideally using the automated algorithms from the spectrometer manufacturer using a cube region of interest placed inside the volume of interest. The line width of the water peak should be recorded. Both the outer-volume saturation and water suppression settings should be carefully checked according to the manufacturers' procedures before proceeding with the acquisition. Ensure the system is on resonance according to the latest voxel-optimized shim and in order to quantify metabolite levels, an un-suppressed reference spectrum should also be acquired.

### 3.10.5 | Analysis and interpretation

LCModel is considered the gold standard for the analysis of 1H-MRS spectra and can provide absolute quantification of a large range of metabolites. Although metabolite levels are often reported as a ratio to total choline or creatine, these metabolite levels may also be changing due to disease pathology and therefore can confound results. As such, wherever possible absolute values should be reported. Metabolites of interest include:

NAA—classically neuronal marker and a marker of neuronal injury—but is also found in oligodendrites/myelin.<sup>113</sup>

Glutamate and glutamine—as their molecular structures are very similar, separating glutamate and glutamine

can be difficult, particularly at lower field strengths and therefore these are often reported as a combined measure “Glx.” Glutamate, localized to neurons, is the brain's most abundant excitatory neurotransmitter. Glutamate is stored as glutamine in glia, and alterations in glutamate-glutamine cycling have been observed in the hippocampus of epilepsy patients.<sup>114</sup> Elevated levels of glutamate lead to increased excitotoxicity. Glutamate is the precursor to both  $\gamma$ -aminobutyric acid (GABA) and glutathione (GSH).<sup>115</sup>

Myo-inositol—specific to glial cells with increases thought to reflect gliosis or hyperosmolarity,<sup>116</sup> Elevated in the brain of patients with temporal lobe epilepsy and hippocampal sclerosis, myo-inositol may allow to distinguish between the focus and seizure spread.<sup>116</sup> Furthermore, myo-inositol was elevated in the pilocarpine poststatus epilepticus rat model. In this model, it predicted which rats developed epilepsy after an acute injury, thus serving as a potential early biomarker of epileptogenesis.<sup>108,110</sup>

### 3.11 | Positron emission tomography and single photon emission computed tomography

CRF File name: 11 CRF module - PET and SPECT imaging.docx

CDE File name: 11 CDE chart - PET and SPECT imaging.xlsx ([Supporting information](#))

### 3.11.1 | Rationale

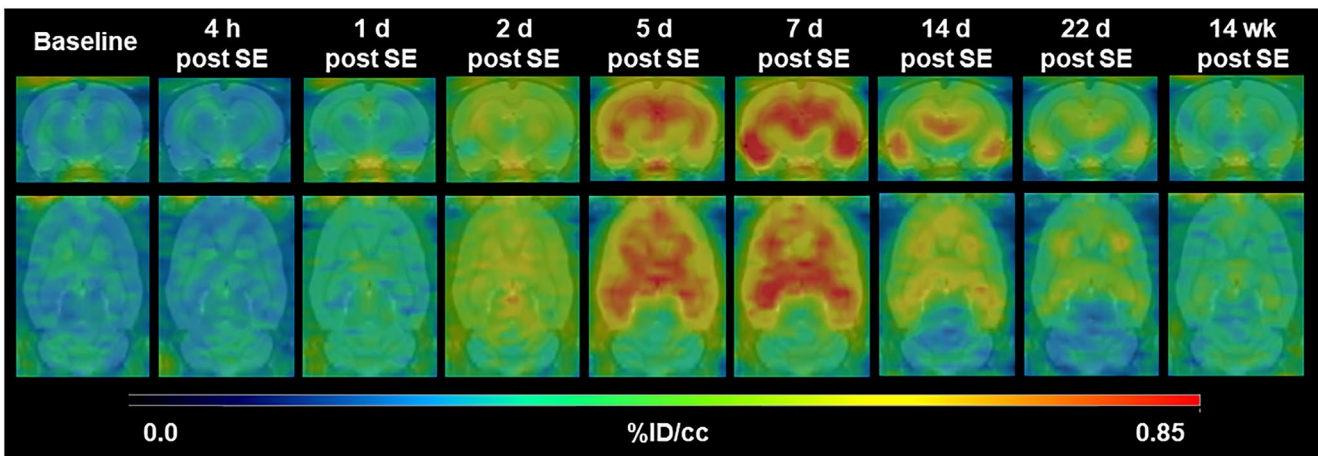
Epilepsies are typically associated with various changes in cerebral cellular and molecular functions. These functions can be analyzed by nuclear in vivo imaging techniques like PET or SPECT using radioisotope-labeled compounds (radiotracers). Due to the relatively short half-life of the most commonly used isotopes, radiotracers are usually labeled in specialized radiochemistry laboratories located close to the imaging site. The laborious process of radiotracer synthesis and the need for a dedicated infrastructure to work with radioactivity in laboratory animals limits the availability of these valuable techniques. Nevertheless, the option to visualize molecular changes associated with brain inflammation (Figure 21), neurotransmission, metabolism, perfusion,

or BBB integrity, as well as the direct clinical translatability makes PET and SPECT important tools in preclinical and clinical epilepsy research.<sup>117–120</sup> In this section, as well as in the accompanying CRF (see also Figure 22), the most important details are described.

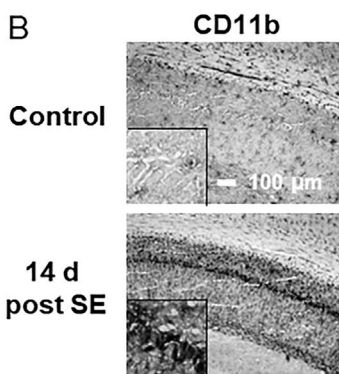
### 3.11.2 | Measurements

Results of dedicated molecular imaging methods are subject to impact by various experimental factors.<sup>121</sup> Furthermore, a broad variety of imaging systems, numerous radiotracers labeled with different isotopes, and various data analysis methods underline the need to standardize the reporting of molecular imaging procedures, particularly to enable the comparison of results originating from

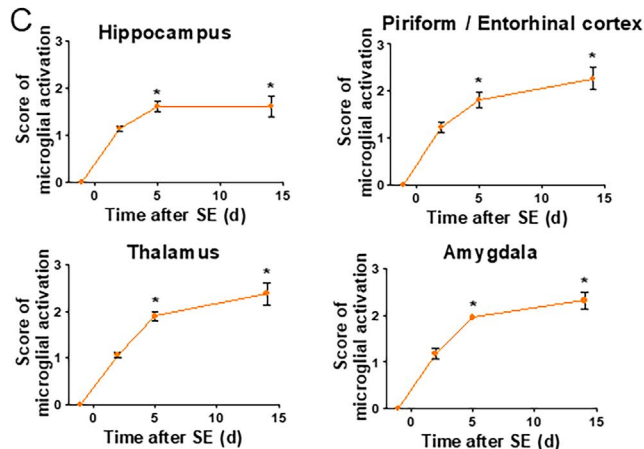
A



B



C



D

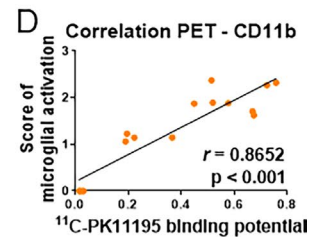


**FIGURE 21** Translocator Protein (TSPO) positron emission tomography (PET) targeting activated microglia during epileptogenesis in rats (systemic pilocarpine poststatus epilepticus (SE) model). (A) Coronal and horizontal brain PET images of [<sup>11</sup>C]PK11195 uptake before and at different time points during epileptogenesis. (B) Microglia staining (CD11b) in control and 14-d post-SE rats (CA1 region of hippocampus; insert displays 4-times-higher magnification of pyramidal cell layer). (C) Semiquantitative evaluation of microglial activation during epileptogenesis. Data are mean ± SEM. Significant changes are indicated by asterisk ( $P < 0.05$ ). (D) Spearman correlation analysis of <sup>11</sup>C-PK11195 in vivo binding potential  $BP_{ND}$  and immunohistochemistry scores. The figure was originally published in the Journal of Nuclear Medicine (Brackhan et al. 2016,<sup>154</sup> © SNMMI).

**Neuroimaging Studies****Case Report Form: 11 CRF - PET and SPECT imaging.docx****CRF module: PET and SPECT imaging**

Date and time that this CRF was filled out:

Name of person filling out CRF:

Project name/Identifier:

Animal ID:

| <b>CDE Name</b>   | <b>Data Collected</b>  |
|---|--|
| Other CRFs to be filled in with regards to a complete data set: CRF1 Technical Information; CRF2 Physiology (H) |  |
| <b>Imaging Modality</b>   |  |
| Imaging modality  | <input type="checkbox"/> PET <input type="checkbox"/> SPECT  |
| <b>Radiotracer</b>  |  |
| Radioisotope  | <input type="checkbox"/> <sup>15</sup> O <input type="checkbox"/> <sup>13</sup> N <input type="checkbox"/> <sup>11</sup> C <input type="checkbox"/> <sup>68</sup> Ga <input type="checkbox"/> <sup>18</sup> F <input type="checkbox"/> <sup>89</sup> Zr<br><input type="checkbox"/> <sup>99m</sup> Tc <input type="checkbox"/> <sup>123</sup> I <input type="checkbox"/> <sup>111</sup> In<br><input type="checkbox"/> Other |
| If other, please specify  |  |
| Imaging target  | <input type="checkbox"/> Metabolism<br><input type="checkbox"/> Perfusion<br><input type="checkbox"/> Neuro-receptors<br><input type="checkbox"/> Inflammation<br><input type="checkbox"/> Blood-brain barrier<br><input type="checkbox"/> Cell tracking<br><input type="checkbox"/> Unknown<br><input type="checkbox"/> Other   |
| If other, please specify  |  |
| Specific radiotracer  |  |
| <b>Imaging protocol</b>   |  |
| Scan protocol   | <input type="checkbox"/> Dynamic   |

**FIGURE 22** PET and SPECT case report form (see main text for details)

different imaging laboratories. Standardization of imaging procedures and analysis itself, as needed for multicenter preclinical studies,<sup>2,122</sup> is a challenge for which the current efforts to standardize reporting might represent the basic first step.

### 3.11.3 | Equipment

- PET and SPECT scanners: Various preclinical nuclear imaging systems are available. Differences in sensitivity, resolution, acquisition settings, or field of view can strongly influence the results of a specific study.<sup>123,124</sup> While the use of dedicated clinical scanners is also possible in principle, the respective resolution has to be considered as insufficient for most epilepsy-related preclinical studies, particularly in mice. Today, most nuclear imaging scanners are multi-modality systems, i.e., they are combined with a second modality like CT

for anatomical co-registration. In recent years, and especially in brain research, MR scanners, combined with PET or SPECT became more common. Importantly, these modalities are not only available as side-by-side systems but also as fully integrated multimodal scanners,<sup>125</sup> allowing simultaneous functional PET/MRI studies.

- Radiotracer: For many imaging targets more than one radiotracer is available, with different target affinity or labeled with different radioisotopes,<sup>17</sup> and it is often difficult to decide which one to establish on-site. Sometimes, new radiotracers with high in vitro target affinity show unwanted unspecific binding when being tested in vivo.<sup>126</sup> The formation of brain-penetrating radiolabeled metabolites with reduced or no target affinity might also impede data interpretation.<sup>127</sup> Furthermore, a molecular change believed to be specific for a certain cell type or pathological situation might also occur in other situations or cell types.<sup>128</sup> The choice of the

|  |  |
|--|--|
|  | <input type="checkbox"/> Static<br><input type="checkbox"/> Unknown  |
| Route of radiotracer administration        | <input type="checkbox"/> Intravenous<br><input type="checkbox"/> Intraperitoneal<br><input type="checkbox"/> Unknown<br><input type="checkbox"/> Other   |
| If other, please specify                   |  |
| Activity dose in MBq                       |  |
| Activity concentration in kBq/ml           |  |
| Specific activity MBq/ $\mu$ g             |  |
| Date/Time of injection of dose             |  |
| Injection volume in ml                     |  |
| Administration protocol                    | <input type="checkbox"/> Bolus injection<br><input type="checkbox"/> Infusion<br><input type="checkbox"/> Unknown<br><input type="checkbox"/> Other  |
| If other, please specify                   |  |
| Scan duration in minutes                   |  |
| Blood sampling                             | <input type="checkbox"/> Full arterial input function;<br><input type="checkbox"/> Single/repeated arterial sample(s);<br><input type="checkbox"/> Single/repeated venous sample(s);<br><input type="checkbox"/> No blood sample(s);<br><input type="checkbox"/> Unknown<br><input type="checkbox"/> Other |
| If other, please specify                   |  |
| Anatomic co-registration scan              | <input type="checkbox"/> CT <input type="checkbox"/> MRI <input type="checkbox"/> None   |
| Individual attenuation correction scan     | <input type="checkbox"/> Yes <input type="checkbox"/> No <input type="checkbox"/> Unknown  |
| <b>Analysis</b>                            |  |
| Analysis software, please specify          |  |
| Image reconstruction and analysis pipeline |  |

**Parameters**

|  |  |
|--|--|
| Imaging date and time                  |  |
| Time Point after initial insult (days) |  |

**Instructions:** Please check boxes where applicable. If none of the predetermined options is appropriate use the default space to specify your answer. This form is to be filled in for one individual animal.

FIGURE 22 (Continued)

radiotracer will also be influenced by the availability of respective precursor molecules and the radioisotopes needed for radiolabeling. For short half-life isotopes like oxygen-15 (~2 min), nitrogen-13 (~10 min), or carbon-11 (~20 min), an on-site cyclotron is a prerequisite for effective radiochemistry, while other cyclotron-generated isotopes like fluorine-18 (~110 min) might be transported over medium distances. Isotopes like gallium-68 (~67 min) or technetium-99m (~6 h) can be produced in on-site generators containing the parent isotope. Longer living isotopes like indium-111 (~67 h)

or zirconium-89 (~78 h) often used for cell or antibody labeling, have no major transport range limitations. The study design and the scientific question will also influence the choice of PET and SPECT isotopes. For preclinical PET, different positron ranges of different isotopes limit the achievable image resolution, which may be crucial when using mouse models. Concerning half-life, the isotope needs to be chosen according to the pharmacokinetic properties of the radiotracer. If the distribution to the target and the elimination from the blood is fast, a short half-life might be desirable. If a molecule

stays in the bloodstream for long periods resulting in high unspecific background values, like antibodies, or cells that should be tracked over days, longer living isotopes might be needed.

### 3.11.4 | Procedure

*Animal state/Preconditioning:* As preclinical nuclear imaging visualizes changes on a molecular level, it is relatively sensitive to external influences, like the time of day, metabolic state, type of anesthesia etc.<sup>121</sup> Therefore, detailed protocols and standardization of parameters are mandatory. Unfortunately, there is no general agreement or validated guideline available for preclinical molecular imaging studies. Nevertheless, various efforts are made to better understand and reduce variability within multicenter imaging studies<sup>2,121,124</sup>

*Anesthesia:* The anesthesia protocol has been identified as a relevant factor in various molecular imaging studies with a focus on [<sup>18</sup>F]FDG PET.<sup>129–131</sup> Unfortunately, for many other nuclear imaging protocols, the influence of anesthesia still remains unclear. Again, there can be no general recommendation on which anesthesia is the best choice for molecular imaging. In recent years, there is a clear trend towards inhalation anesthesia with isoflurane as the most commonly used anesthetic. Inhalation anesthesia has the advantage that depth is adjustable, and the duration of anesthesia is principally not limited. Nevertheless, the impact on molecular imaging outcome parameters probably increases as a function of anesthesia length. Furthermore, the influence of isoflurane, e.g., on brain perfusion has been described,<sup>132</sup> and there is also evidence of therapeutic effects of repetitive isoflurane anesthesia.<sup>24</sup>

*Scan protocol:* The choice for the type of acquisition (dynamic or static) highly depends on the intended analysis method for the respective imaging data. The gold standard, i.e., full kinetic modeling with individual arterial input functions, is usually not possible in longitudinal preclinical studies. Shorter protocols based on static scans with an uptake phase between radiotracer injection and acquisition facilitate higher throughput, which might be desirable for a laborious and expensive technique like nuclear imaging. Nevertheless, all efforts for more simplified protocols need to be carefully validated in healthy animals and disease models before being used for bigger cohorts.

The most commonly used radiotracer administration route in laboratory rodents is intravenous injection via the lateral tail vein. If trained properly, high success rates well above 90% are not only possible<sup>133</sup> but also needed to avoid high drop-out rates in longitudinal studies. Alternative administration routes such as intraperitoneal

injections might be chosen under specific circumstances but will considerably influence the pharmacokinetics and therefore also the choice of the analysis method, as most kinetic models are based on intravenous bolus injection. Another option is the application of infusion protocols, which might be used to reach steady-state radiotracer blood levels in order to directly obtain kinetic parameters.<sup>134</sup>

Activity doses required for sufficient image quality will be highly dependent on the applied radiotracer and the type of nuclear scanner. Usually, higher amounts of activity are needed for SPECT imaging as collimators are part of the scanners, which allow only limited amounts of the radiation reaching the detectors. Especially for longitudinal studies, one must also keep in mind that injected amounts of radioactivity might reach levels that result in systemic effects.<sup>135</sup>

The injection volume of radiotracers is a parameter that is sometimes problematic in laboratory animals, particularly in mice. If radiotracers are also used for clinical applications, the radioactivity concentration might be relatively low, potentially resulting in too high application volumes for preclinical use. Recommendations and various guidelines for applications in laboratory rodents limit amounts of maximal volumes for intravenous injection, and severe systemic effects might occur when injecting higher volumes.<sup>136</sup> Thus, specific radiotracer preparation for preclinical use resulting in small volumes needs to be achieved beforehand.

As indicated in the preceding text, blood sampling might be needed for some kinetic models. In laboratory rodents, (arterial) blood sampling is limited due to the invasiveness of the sampling procedure, blood volume, and accessibility of animals during the scan. Instead of arterial blood sampling, venous samples might also be considered after proper validation, and also single blood samples can be of value to adapt population-based blood curves for single animals.<sup>137</sup> Alternatively, an image-derived input function (IDIF) might be extracted from the imaging datasets during data analysis.<sup>137</sup>

Anatomical co-registration using CT or MRI is often included in molecular imaging protocols as correct positioning of regions of interest is crucial for reliable data analysis, but difficult to achieve in case the analysis is solely based on the nuclear scan. For anatomical co-registration, short MRI or low-dose CT scans are usually sufficient. Particularly for longitudinal studies, including multiple imaging time points, the potential impact of cumulating radiation doses needs to be considered when using CT for co-registration.<sup>138,139</sup>

Attenuation correction accounts for the interaction of radioactive irradiation with the tissue. There is increasing evidence that it should be applied even to mouse scans.<sup>140</sup>

The most usual methods to obtain a transmission scan are to apply a CT scan or to use, e.g., a cobalt-57 transmission source. More recently, setups were established to use also MRI data for attenuation correction.<sup>141</sup> If this is done on an individual basis it will add some time to the total scan duration. In the case that animals are reproducibly positioned and of comparable weight, population transmission scans might also be acquired independently from the individual scan, therefore facilitating throughput.

### 3.11.5 | Analysis and interpretation

Information on data reconstruction used in the specific scanner software needs to be considered and included in the analysis pipeline description. The software used for data analysis represents another important parameter that might provide various analysis options. Data analysis of (preclinical) nuclear imaging studies is complex and needs to be adapted to the individual study.<sup>17</sup> The chosen imaging protocol already strongly determines the options for data analysis. There is no general guideline on how to choose the optimal analysis approach, and respective methods are under constant development and improvement. To account for individual variation, reference regions might be included in the data analysis. Atlas-based regional analysis is often applied to generate different types of standardized uptake values or to perform kinetic modeling (using a reference tissue method, blood input functions, or IDIF). In addition, the generation of parametric maps for uptake or kinetic data might be highly useful. Without doubt, each method needs proper validation beforehand. In the context of this CRF module, it seems not possible to account for all options available for data analysis. Nevertheless, at least a detailed analysis pipeline should be given.

## 4 | DISCUSSION

It is hoped that the detailed case report forms (CRFs) and common data elements (CDEs) provided with this manuscript will aid existing cross-laboratory collaborations, and even provide the impetus to stimulate further collaborative efforts to acquire large datasets of size and complexity required to solve problems that are too large for any single laboratory alone. The current increasing trend toward the funding of multiple laboratories for preclinical projects over multiple academic centers both nationally and internationally for epilepsy (EpiBioS4Rx Center without Walls, NIH) and for traumatic brain injury biomarkers (Translational Outcome Project in Neurotrauma, TopNT NIH) has already given rise to the adaptation of

protocols for harmonization of preclinical data acquisition and processing among centers. While the work is ongoing and beginning to yield fruit,<sup>2,142,143</sup> the harmonization procedures are continuing to evolve.

A challenge yet to be addressed for multicenter MRI research is the absence of any standard preclinical phantoms to facilitate internal calibration of signal quality, and serving as a possible external control for detecting variation in proton relaxation times and signal quality across laboratories with spectrometers operating at the same field strength. Of not trivial importance allied to this issue, is the creation of a standardized, diffusion weighting imaging phantom with a fiber size small enough to simulate axon diameters in the rodent brain. Additionally, the problem of combining data obtained at different field strengths, and the inherent differences in relaxation times and signal sensitivity that it brings, has yet to be sufficiently solved. Current practice requires the use of sham controls to create a population-based statistical analysis at each field strength from which to identify signal abnormalities relate to disease progression for final combination across the centers.

The attached CDEs and CRFs are biased toward image acquisition and general analytics pipelines with fewer technical details of analysis provided, apart from the general suggestions within each result section. This was done intentionally since the preclinical field has yet to arrive at a consensus with regard to standard processing pipelines. While a large number of published manuscripts follow clinical methods to some degree, methods diverge due to the different brain anatomy or physiology within preclinical species and compared to that of the human brain. We suggest that current efforts by preclinical consortia (EpiBios4Rx, TOPNT) to generate multi-site data, together with the recent initiative by the US Veterans Affairs to create an Interagency Resource Coordinating Center (IRCC) for Preclinical TBI Research focusing on CDEs, will act to strengthen preclinical CDEs efforts and extend into additional areas such as analytical pipelines.

In the field of nuclear imaging, and particularly for PET, generating quantitative data has always been a major goal. Therefore, manufacturers agreed early on the standardized NEMA phantom to compare systems performances of different preclinical PET imaging systems.<sup>144</sup> Nevertheless, two recent publications showed that both imaging system-based variation (including reconstruction algorithms) and laboratory-specific imaging procedures lead to an immense inter-laboratory variation of imaging data.<sup>124,145</sup> Potential sources of variation are diverse and might include environmental factors such as room temperature, humidity or light conditions during the scan, transport conditions between animal facilities and scanning areas, animal sources, anesthesia equipment, and many more. Reassuringly, both publications indicate, that

harmonization of procedures can lead to decreased variation and principally enables multicenter nuclear imaging studies, but they also show that more research is needed to fully understand the sources of variation of data obtained at different imaging sites. The recent development of preclinical (and clinical) simultaneous PET/MRI scanners<sup>125</sup> and their commercial availability will further enable the generation of subject-individual multimodal datasets and also foster the need for imaging standardization including multiple modalities.

The significant utility of preclinical MRI or nuclear imaging is not merely confined to the acquisition of multiple, longitudinal imaging snapshots of disease progression and identification of early biomarkers for epilepsy. The bridge to the clinic that it provides via clinical research imaging is a significant factor that raises the possibility of not just simply allowing forward clinical translation of new techniques and preclinically identified biomarkers but allowing for the possibility of reverse translation to validate existing preclinical models for clinical relevance, and giving rise to newer models informed directly from clinical work. The continued prevalence of this highly flexible research modality is ensured by recent publications showing the potential of combining calcium imaging or electrophysiology with MRI for simultaneous acquisition of signals at multiple spatiotemporal scales and signal sources.<sup>146–148</sup> Given the significant potential of multiscale data for informing on brain networks at the cellular level, and by correlation, diagnosing simultaneous acquired MRI or PET imaging voxel-based signals for physiologically relevant phenomena, the stage appears set for a continued flow of clinically translatable information from preclinical imaging studies. Also relevant to this combinatorial, technological arsenal is the employment of chemogenetics to manipulate circuits, with readout by all preclinical imaging modalities in order to assign causality to network-level events.<sup>149,150</sup> These and other developing technologies were not covered for combinatorial use within the currently written CRFs. However, the sheer size and complexity of these newly combined datasets as well as the pace of technological innovation, suggests that continued effort is required for developing CDEs and CRFs to meet future demands for multi-site collaboration at the scale of 4 and 5-dimensional dataset acquisition.

## ACKNOWLEDGMENTS

This report was written by experts selected by the International League Against Epilepsy (ILAE) and the American Epilepsy Society (AES) and was approved for publication by the ILAE and the AES. Opinions expressed by the authors, however, do not represent the policy or position of the ILAE or the AES. We are also grateful to the AES and ILAE for their financial support of the activities

of TASK3 working groups. We are grateful to Dr Lauren Harte-Hargrove, director of research at CURE Epilepsy, and Victoria A. Marciniak from the Cardinal Gibbons High School at Raleigh North Carolina, for their expert work in converting the CRFs to the CDE spreadsheets.

## CONFLICT OF INTEREST

Alon Friedman is Associate Editor for *Epilepsia Open*. None of the authors has any conflict of interest to disclose. We confirm that we have read the Journal's position on issues involved in ethical publication and affirm that this report is consistent with those guidelines.

## ORCID

Erwin A. van Vliet  <https://orcid.org/0000-0001-5747-3202>

Ofer Prager  <https://orcid.org/0000-0002-0172-0849>

Alon Friedman  <https://orcid.org/0000-0003-4780-8456>

Jens P. Bankstahl  <https://orcid.org/0000-0003-4735-4490>

David K. Wright  <https://orcid.org/0000-0002-7535-8651>

Terence J. O'Brien  <https://orcid.org/0000-0002-7198-8621>

Heidrun Potschka  <https://orcid.org/0000-0003-1506-0252>

Olli Gröhn  <https://orcid.org/0000-0003-1372-1651>

Neil G. Harris  <https://orcid.org/0000-0002-1965-6750>

## REFERENCES

1. Wilkinson MD, Dumontier M, Aalbersberg IJ, Appleton G, Axton M, Baak A, et al. The FAIR Guiding Principles for scientific data management and stewardship. *Sci Data*. 2016;3:160018.
2. Immonen R, Smith G, Brady RD, Wright D, Johnston L, Harris NG, et al. Harmonization of pipeline for preclinical multicenter MRI biomarker discovery in a rat model of post-traumatic epileptogenesis. *Epilepsy Res*. 2019;150:46–57.
3. Harte-Hargrove LC, French JA, Pitkanen A, Galanopoulou AS, Whittemore V, Scharfman HE. Common data elements for preclinical epilepsy research: standards for data collection and reporting. A TASK3 report of the AES/ILAE Translational Task Force of the ILAE. *Epilepsia*. 2017;58(Suppl 4):78–86.
4. Harte-Hargrove LC, Galanopoulou AS, French JA, Pitkanen A, Whittemore V, Scharfman HE. Common data elements (CDEs) for preclinical epilepsy research: introduction to CDEs and description of core CDEs. A TASK3 report of the ILAE/AES joint translational task force. *Epilepsia Open*. 2018;3:13–23.
5. Barker-Haliski M, Harte-Hargrove LC, Ravizza T, Smolders I, Xiao B, Brandt C, et al. A companion to the preclinical common data elements for pharmacologic studies in animal models of seizures and epilepsy. A Report of the TASK3 Pharmacology Working Group of the ILAE/AES Joint Translational Task Force. *Epilepsia Open*. 2018;3:53–68.

6. Gorter JA, van Vliet EA, Dedeurwaerdere S, Buchanan GF, Friedman D, Borges K, et al. A companion to the preclinical common data elements for physiologic data in rodent epilepsy models. A report of the TASK3 Physiology Working Group of the ILAE/AES Joint Translational Task Force. *Epilepsia Open*. 2018;3:69–89.
7. Mazarati A, Jones NC, Galanopoulou AS, Harte-Hargrove LC, Kalynchuk LE, Lenck-Santini PP, et al. A companion to the preclinical common data elements on neurobehavioral comorbidities of epilepsy: a report of the TASK3 behavior working group of the ILAE/AES Joint Translational Task Force. *Epilepsia Open*. 2018;3:24–52.
8. Ono T, Wagenaar J, Giorgi FS, Fabera P, Hanaya R, Jefferys J, et al. A companion to the preclinical common data elements and case report forms for rodent EEG studies. A report of the TASK3 EEG Working Group of the ILAE/AES Joint Translational Task Force. *Epilepsia Open*. 2018;3:90–103.
9. Lapinlampi N, Melin E, Aronica E, Bankstahl JP, Becker A, Bernard C, et al. Common data elements and data management: remedy to cure underpowered preclinical studies. *Epilepsy Res*. 2017;129:87–90.
10. Bertoglio D, Verhaeghe J, Dedeurwaerdere S, Grohn O. Neuroimaging in animal models of epilepsy. *Neuroscience*. 2017;358:277–99.
11. Reimann HM, Niendorf T. The (Un)Conscious mouse as a model for human brain functions: key principles of anesthesia and their impact on translational neuroimaging. *Front Syst Neurosci*. 2020;14:8.
12. Tremoleda JL, Kerton A, Gsell W. Anaesthesia and physiological monitoring during in vivo imaging of laboratory rodents: considerations on experimental outcomes and animal welfare. *EJNMMI Res*. 2012;2:44.
13. Paasonen J, Salo RA, Shatillo A, Forsberg MM, Narvainen J, Huttunen JK, et al. Comparison of seven different anesthesia protocols for nicotine pharmacologic magnetic resonance imaging in rat. *Eur Neuropsychopharmacol*. 2016;26:518–31.
14. Paasonen J, Stenroos P, Salo RA, Kiviniemi V, Grohn O. Functional connectivity under six anesthesia protocols and the awake condition in rat brain. *Neuroimage*. 2018;172:9–20.
15. Airaksinen AM, Niskanen JP, Chamberlain R, Huttunen JK, Nissinen J, Garwood M, et al. Simultaneous fMRI and local field potential measurements during epileptic seizures in medetomidine-sedated rats using raser pulse sequence. *Magn Reson Med*. 2010;64:1191–9.
16. Liu X, Zhu XH, Zhang Y, Chen W. Neural origin of spontaneous hemodynamic fluctuations in rats under burst-suppression anesthesia condition. *Cereb Cortex*. 2011;21:374–84.
17. Kiessling F, Pichler BJ, Hauff P. *Small Animal Imaging: Basics and Practical Guide*. Cham: Springer International Publishing; 2017.
18. Weber R, Ramos-Cabrer P, Wiedermann D, van Camp N, Hoehn M. A fully noninvasive and robust experimental protocol for longitudinal fMRI studies in the rat. *Neuroimage*. 2006;29:1303–10.
19. Huttunen JK, Grohn O, Penttonen M. Coupling between simultaneously recorded BOLD response and neuronal activity in the rat somatosensory cortex. *Neuroimage*. 2008;39:775–85.
20. Zhurakovskaya E, Paasonen J, Shatillo A, Lipponen A, Salo R, Aliev R, et al. Global functional connectivity differences between sleep-like states in urethane anesthetized rats measured by fMRI. *PLoS One*. 2016;11:e0155343.
21. Stenroos P, Paasonen J, Salo RA, Jokivarsi K, Shatillo A, Tanila H, et al. Awake rat brain functional magnetic resonance imaging using standard radio frequency coils and a 3D printed restraint kit. *Front Neurosci*. 2018;12:548.
22. Flecknell P. In: Flecknell P, editor. *Laboratory Animal Anaesthesia*. Oxford: Academic Press; 2016.
23. Lohrke J, Frenzel T, Endrikat J, Alves FC, Grist TM, Law M, et al. 25 years of contrast-enhanced MRI: developments, current challenges and future perspectives. *Adv Ther*. 2016;33:1–28.
24. Bar-Klein G, Klee R, Brandt C, Bankstahl M, Bascunana P, Tollner K, et al. Isoflurane prevents acquired epilepsy in rat models of temporal lobe epilepsy. *Ann Neurol*. 2016;80:896–908.
25. van Vliet EA, Otte WM, Gorter JA, Dijkhuizen RM, Wadman WJ. Longitudinal assessment of blood–brain barrier leakage during epileptogenesis in rats. A quantitative MRI study. *Neurobiol Dis*. 2014;63:74–84.
26. Nagaraja TN, Karki K, Ewing JR, Divine GW, Fenstermacher JD, Patlak CS, et al. The MRI-measured arterial input function resulting from a bolus injection of Gd-DTPA in a rat model of stroke slightly underestimates that of Gd-[14C] DTPA and marginally overestimates the blood-to-brain influx rate constant determined by Patlak plots. *Magn Reson Med*. 2010;63:1502–9.
27. Nagaraja TN, Nagesh V, Ewing JR, Whitton PA, Fenstermacher JD, Knight RA. Step-down infusions of Gd-DTPA yield greater contrast-enhanced magnetic resonance images of BBB damage in acute stroke than bolus injections. *Magn Reson Imaging*. 2007;25:311–8.
28. Knight RA, Karki K, Ewing JR, Divine GW, Fenstermacher JD, Patlak CS, et al. Estimating blood and brain concentrations and blood-to-brain influx by magnetic resonance imaging with step-down infusion of Gd-DTPA in focal transient cerebral ischemia and confirmation by quantitative autoradiography with Gd-[(14C)DTPA. *J Cereb Blood Flow Metab*. 2009;29:1048–58.
29. Veksler R, Vazana U, Serlin Y, Prager O, Ofer J, Shemen N, et al. Slow blood-to-brain transport underlies enduring barrier dysfunction in American football players. *Brain*. 2020;143:1826–42.
30. Heye AK, Culling RD, Valdes Hernandez Mdel C, Thrippleton MJ, Wardlaw JM. Assessment of blood-brain barrier disruption using dynamic contrast-enhanced MRI. A systematic review. *Neuroimage Clin*. 2014;6:262–74.
31. Bar-Klein G, Lublinsky S, Kamintsky L, Noyman I, Veksler R, Dalipaj H, et al. Imaging blood-brain barrier dysfunction as a biomarker for epileptogenesis. *Brain*. 2017;140:1692–705.
32. Kermodé AG, Tofts PS, Thompson AJ, MacManus DG, Rudge P, Kendall BE, et al. Heterogeneity of blood-brain barrier changes in multiple sclerosis: an MRI study with gadolinium-DTPA enhancement. *Neurology*. 1990;40:229–35.
33. Milikovsky DZ, Ofer J, Senatorov VV Jr, Friedman AR, Prager O, Sheintuch L, et al. Paroxysmal slow cortical activity in Alzheimer's disease and epilepsy is associated with blood-brain barrier dysfunction. *Sci Transl Med*. 2019;11:eaaw8954.

34. Roch C, Leroy C, Nehlig A, Namer JJ. Magnetic resonance imaging in the study of the lithium-pilocarpine model of temporal lobe epilepsy in adult rats. *Epilepsia*. 2002;43:325–35.
35. Boullieret V, Boyet S, Marescaux C, Nehlig A. Mapping of the progressive metabolic changes occurring during the development of hippocampal sclerosis in a model of mesial temporal lobe epilepsy. *Brain Res*. 2000;852:255–62.
36. Tomkins O, Friedman O, Ivens S, Reiffurth C, Major S, Dreier JP, et al. Blood-brain barrier disruption results in delayed functional and structural alterations in the rat neocortex. *Neurobiol Dis*. 2007;25:367–77.
37. van Vliet EA, Otte WM, Wadman WJ, Aronica E, Kooij G, de Vries HE, et al. Blood-brain barrier leakage after status epilepticus in rapamycin-treated rats I: magnetic resonance imaging. *Epilepsia*. 2016;57:59–69.
38. Bankstahl M, Breuer H, Leiter I, Markel M, Bascunana P, Michalski D, et al. Blood-brain barrier leakage during early epileptogenesis is associated with rapid remodeling of the neurovascular unit. *eNeuro*. 2018;5:ENEURO.0123-18.2018.
39. Breuer H, Meier M, Schneefeld S, Hartig W, Wittneben A, Markel M, et al. Multimodality imaging of blood-brain barrier impairment during epileptogenesis. *J Cereb Blood Flow Metab*. 2017;37:2049–61.
40. Hanael E, Veksler R, Friedman A, Bar-Klein G, Senatorov VV Jr, Kaufer D, et al. Blood-brain barrier dysfunction in canine epileptic seizures detected by dynamic contrast-enhanced magnetic resonance imaging. *Epilepsia*. 2019;60:1005–16.
41. Chassidim Y, Veksler R, Lublinsky S, Pell GS, Friedman A, Shelef I. Quantitative imaging assessment of blood-brain barrier permeability in humans. *Fluids Barriers CNS*. 2013;10:9.
42. Veksler R, Shelef I, Friedman A. Blood-brain barrier imaging in human neuropathologies. *Arch Med Res*. 2014;45:646–52.
43. Weissberg I, Veksler R, Kamintsky L, Saar-Ashkenazy R, Milikovsky DZ, Shelef I, et al. Imaging blood-brain barrier dysfunction in football players. *JAMA Neurol*. 2014;71:1453–5.
44. Ruber T, David B, Luchters G, Nass RD, Friedman A, Surges R, et al. Evidence for peri-ictal blood-brain barrier dysfunction in patients with epilepsy. *Brain*. 2018;141:2952–65.
45. Tomkins O, Feintuch A, Benifla M, Cohen A, Friedman A, Shelef I. Blood-brain barrier breakdown following traumatic brain injury: a possible role in posttraumatic epilepsy. *Cardiovasc Psychiatry Neurol*. 2011;2011:765923.
46. Tomkins O, Kaufer D, Korn A, Shelef I, Golan H, Reichenthal E, et al. Frequent blood-brain barrier disruption in the human cerebral cortex. *Cell Mol Neurobiol*. 2001;21:675–91.
47. Tomkins O, Shelef I, Kaizerman I, Eliushin A, Afawi Z, Misk A, et al. Blood-brain barrier disruption in post-traumatic epilepsy. *J Neurol Neurosurg Psychiatry*. 2008;79:774–7.
48. Prager O, Chassidim Y, Klein C, Levi H, Shelef I, Friedman A. Dynamic in vivo imaging of cerebral blood flow and blood-brain barrier permeability. *Neuroimage*. 2010;49:337–44.
49. Vazana U, Veksler R, Pell GS, Prager O, Fassler M, Chassidim Y, et al. Glutamate-mediated blood-brain barrier opening: implications for neuroprotection and drug delivery. *J Neurosci*. 2016;36:7727–39.
50. Prager O, Kamintsky L, Hasam-Henderson LA, Schoknecht K, Wuntke V, Papageorgiou I, et al. Seizure-induced microvascular injury is associated with impaired neurovascular coupling and blood-brain barrier dysfunction. *Epilepsia*. 2019;60:322–36.
51. Kumamaru KK, Hoppel BE, Mather RT, Rybicki FJ. CT angiography: current technology and clinical use. *Radiol Clin North Am*. 2010;48(213-235):vii.
52. Hurford R, Wolters FJ, Li L, Lau KK, Kuker W, Rothwell PM. Prognosis of asymptomatic intracranial stenosis in patients with transient ischemic attack and minor stroke. *JAMA Neurol*. 2020;77:947–54.
53. Schoknecht K, Kikhia M, Lemale CL, Liotta A, Lublinsky S, Mueller S, et al. The role of spreading depolarizations and electrographic seizures in early injury progression of the rat photothrombosis stroke model. *J Cereb Blood Flow Metab*. 2020;41:413–30.
54. Schoknecht K, Prager O, Vazana U, Kamintsky L, Harhausen D, Zille M, et al. Monitoring stroke progression: in vivo imaging of cortical perfusion, blood-brain barrier permeability and cellular damage in the rat photothrombosis model. *J Cereb Blood Flow Metab*. 2014;34:1791–801.
55. Debrey SM, Yu H, Lynch JK, Lovblad KO, Wright VL, Janket SJ, et al. Diagnostic accuracy of magnetic resonance angiography for internal carotid artery disease: a systematic review and meta-analysis. *Stroke*. 2008;39:2237–48.
56. Westerlaan HE, van Dijk JM, Jansen-van der Weide MC, de Groot JC, Groen RJ, Mooij JJ, et al. Intracranial aneurysms in patients with subarachnoid hemorrhage: CT angiography as a primary examination tool for diagnosis—systematic review and meta-analysis. *Radiology*. 2011;258:134–45.
57. Teixeira OU, Bortolotto LA, Silva HB. The contrast-enhanced Doppler ultrasound with perfluorocarbon exposed sonicated albumin does not improve the diagnosis of renal artery stenosis compared with angiography. *J Negat Results Biomed*. 2004;3:3.
58. Sugita K, Kamida T, Matsuta H, Shimomura T, Fujiki M. Usefulness of pulsed arterial spin-labeling MRI for localizing a seizure focus: a surgical case. *Seizure*. 2014;23:318–20.
59. Choy M, Wells JA, Thomas DL, Gadian DG, Scott RC, Lythgoe MF. Cerebral blood flow changes during pilocarpine-induced status epilepticus activity in the rat hippocampus. *Exp Neurol*. 2010;225:196–201.
60. Hayward NM, Tuunanen PI, Immonen R, Nnode-Ekane XE, Pitkanen A, Grohn O. Magnetic resonance imaging of regional hemodynamic and cerebrovascular recovery after lateral fluid-percussion brain injury in rats. *J Cereb Blood Flow Metab*. 2011;31:166–77.
61. Kim SG. Quantification of relative cerebral blood flow change by flow-sensitive alternating inversion recovery (FAIR) technique: application to functional mapping. *Magn Reson Med*. 1995;34:293–301.
62. Alsop DC, Detre JA, Golay X, Gunther M, Hendrikse J, Hernandez-Garcia L, et al. Recommended implementation of arterial spin-labeled perfusion MRI for clinical applications: a consensus of the ISMRM perfusion study group and the European consortium for ASL in dementia. *Magn Reson Med*. 2015;73:102–16.
63. Sicard K, Shen Q, Brevard ME, Sullivan R, Ferris CF, King JA, et al. Regional cerebral blood flow and BOLD responses in conscious and anesthetized rats under basal and hypercapnic conditions: implications for functional MRI studies. *J Cereb Blood Flow Metab*. 2003;23:472–81.

64. Salo RA, Miettinen T, Laitinen T, Grohn O, Sierra A. Diffusion tensor MRI shows progressive changes in the hippocampus and dentate gyrus after status epilepticus in rat - histological validation with Fourier-based analysis. *Neuroimage*. 2017;152:221–36.
65. Sierra A, Laitinen T, Lehtimäki K, Rieppo L, Pitkanen A, Grohn O. Diffusion tensor MRI with tract-based spatial statistics and histology reveals undiscovered lesioned areas in kainate model of epilepsy in rat. *Brain Struct Funct*. 2011;216:123–35.
66. Yankam Njiwa J, Costes N, Bouillot C, Bouvard S, Fieus S, Becker G, et al. Quantitative longitudinal imaging of activated microglia as a marker of inflammation in the pilocarpine rat model of epilepsy using [(11)C]- (R)-PK11195 PET and MRI. *J Cereb Blood Flow Metab*. 2017;37:1251–63.
67. van Luijtelaar G, Mishra AM, Edelbroek P, Coman D, Frankenmolen N, Schaapsmeeders P, et al. Anti-epileptogenesis: Electrophysiology, diffusion tensor imaging and behavior in a genetic absence model. *Neurobiol Dis*. 2013;60:126–38.
68. Hui ES, Cheung MM, Chan KC, Wu EX. B-value dependence of DTI quantitation and sensitivity in detecting neural tissue changes. *Neuroimage*. 2010;49:2366–74.
69. Jones DK, Knosche TR, Turner R. White matter integrity, fiber count, and other fallacies: the do's and don'ts of diffusion MRI. *Neuroimage*. 2013;73:239–54.
70. Andersson JL, Skare S, Ashburner J. How to correct susceptibility distortions in spin-echo-planar images: application to diffusion tensor imaging. *Neuroimage*. 2003;20:870–88.
71. Galovic M, van Dooren VQH, Postma T, Vos SB, Caciagli L, Borzi G, et al. Progressive cortical thinning in patients with focal epilepsy. *JAMA Neurol*. 2019;76:1230–9.
72. Alvim MK, Coan AC, Campos BM, Yasuda CL, Oliveira MC, Morita ME, et al. Progression of gray matter atrophy in seizure-free patients with temporal lobe epilepsy. *Epilepsia*. 2016;57:621–9.
73. Natsume J, Bernasconi N, Andermann F, Bernasconi A. MRI volumetry of the thalamus in temporal, extratemporal, and idiopathic generalized epilepsy. *Neurology*. 2003;60:1296–300.
74. Yoo JG, Jakabek D, Ljung H, Velakoulis D, van Westen D, Looi JCL, et al. MRI morphology of the hippocampus in drug-resistant temporal lobe epilepsy: shape inflation of left hippocampus and correlation of right-sided hippocampal volume and shape with visuospatial function in patients with right-sided TLE. *J Clin Neurosci*. 2019;67:68–74.
75. Jackson GD, Berkovic SF, Duncan JS, Connelly A. Optimizing the diagnosis of hippocampal sclerosis using MR imaging. *AJNR Am J Neuroradiol*. 1993;14:753–62.
76. Vos SB, Winston GP, Goodkin O, Pemberton HG, Barkhof F, Prados F, et al. Hippocampal profiling: localized magnetic resonance imaging volumetry and T2 relaxometry for hippocampal sclerosis. *Epilepsia*. 2020;61:297–309.
77. Kharatishvili I, Sierra A, Immonen RJ, Grohn OH, Pitkanen A. Quantitative T2 mapping as a potential marker for the initial assessment of the severity of damage after traumatic brain injury in rat. *Exp Neurol*. 2009;217:154–64.
78. Manninen E, Chary K, Lapinlampi N, Andrade P, Paananen T, Sierra A, et al. Early increase in cortical T2 relaxation is a prognostic biomarker for the evolution of severe cortical damage, but not for epileptogenesis, after experimental traumatic brain injury. *J Neurotrauma*. 2020;37:2580–94.
79. Choy M, Cheung KK, Thomas DL, Gadian DG, Lythgoe MF, Scott RC. Quantitative MRI predicts status epilepticus-induced hippocampal injury in the lithium-pilocarpine rat model. *Epilepsy Res*. 2010;88:221–30.
80. Dube C, Yu H, Nalcioglu O, Baram TZ. Serial MRI after experimental febrile seizures: altered T2 signal without neuronal death. *Ann Neurol*. 2004;56:709–14.
81. Lehto LJ, Sierra A, Corum CA, Zhang J, Idiyatullin D, Pitkanen A, et al. Detection of calcifications in vivo and ex vivo after brain injury in rat using SWIFT. *Neuroimage*. 2012;61:761–72.
82. Woolrich MW, Jbabdi S, Patenaude B, Chappell M, Makni S, Behrens T, et al. Bayesian analysis of neuroimaging data in FSL. *Neuroimage*. 2009;45:S173–86.
83. Smith SM, Jenkinson M, Woolrich MW, Beckmann CF, Behrens TE, Johansen-Berg H, et al. Advances in functional and structural MR image analysis and implementation as FSL. *Neuroimage*. 2004;23(Suppl 1):S208–19.
84. Avants BB, Tustison NJ, Wu J, Cook PA, Gee JC. An open source multivariate framework for n-tissue segmentation with evaluation on public data. *Neuroinformatics*. 2011;9:381–400.
85. Yushkevich PA, Piven J, Hazlett HC, Smith RG, Ho S, Gee JC, et al. User-guided 3D active contour segmentation of anatomical structures: significantly improved efficiency and reliability. *Neuroimage*. 2006;31:1116–28.
86. Feo R, Giove F. Towards an efficient segmentation of small rodents brain: a short critical review. *J Neurosci Methods*. 2019;323:82–9.
87. Immonen RJ, Kharatishvili I, Sierra A, Einula C, Pitkanen A, Grohn OH. Manganese enhanced MRI detects mossy fiber sprouting rather than neurodegeneration, gliosis or seizure-activity in the epileptic rat hippocampus. *Neuroimage*. 2008;40:1718–30.
88. Nairismagi J, Pitkanen A, Narkilahti S, Huttunen J, Kauppinen RA, Grohn OH. Manganese-enhanced magnetic resonance imaging of mossy fiber plasticity in vivo. *Neuroimage*. 2006;30:130–5.
89. Soria G, Wiedermann D, Justicia C, Ramos-Cabrer P, Hoehn M. Reproducible imaging of rat corticothalamic pathway by longitudinal manganese-enhanced MRI (L-MEMRI). *Neuroimage*. 2008;41:668–74.
90. Tucciarone J, Chuang KH, Dodd SJ, Silva A, Pelled G, Koretsky AP. Layer specific tracing of corticocortical and thalamocortical connectivity in the rodent using manganese enhanced MRI. *Neuroimage*. 2009;44:923–31.
91. Silva AC, Lee JH, Wu CW, Tucciarone J, Pelled G, Aoki I, et al. Detection of cortical laminar architecture using manganese-enhanced MRI. *J Neurosci Methods*. 2008;167:246–57.
92. Aoki I, Tanaka C, Takegami T, Ebisu T, Umeda M, Fukunaga M, et al. Dynamic activity-induced manganese-dependent contrast magnetic resonance imaging (DAIM MRI). *Magn Reson Med*. 2002;48:927–33.
93. Weng JC, Chen JH, Yang PF, Tseng WY. Functional mapping of rat barrel activation following whisker stimulation using activity-induced manganese-dependent contrast. *Neuroimage*. 2007;36:1179–88.
94. Schroeder MP, Weiss C, Procissi D, Wang L, Disterhoft JF. Activity-induced manganese-dependent MRI (AIM-MRI) and

- functional MRI in awake rabbits during somatosensory stimulation. *Neuroimage*. 2016;126:72–80.
95. Tambalo S, Daducci A, Fiorini S, Boschi F, Mariani M, Marinone M, et al. Experimental protocol for activation-induced manganese-enhanced MRI (AIM-MRI) based on quantitative determination of Mn content in rat brain by fast T1 mapping. *Magn Reson Med*. 2009;62:1080–4.
  96. Silva AC, Lee JH, Aoki I, Koretsky AP. Manganese-enhanced magnetic resonance imaging (MEMRI): methodological and practical considerations. *NMR Biomed*. 2004;17:532–43.
  97. Pautler RG. Biological applications of manganese-enhanced magnetic resonance imaging. *Methods Mol Med*. 2006;124:365–86.
  98. Pautler RG, Silva AC, Koretsky AP. In vivo neuronal tract tracing using manganese-enhanced magnetic resonance imaging. *Magn Reson Med*. 1998;40:740–8.
  99. Bock NA, Paiva FF, Silva AC. Fractionated manganese-enhanced MRI. *NMR Biomed*. 2008;21:473–8.
  100. Paasonen J, Laakso H, Pirttimaki T, Stenroos P, Salo RA, Zhurakovskaya E, et al. Multi-band SWIFT enables quiet and artefact-free EEG-fMRI and awake fMRI studies in rat. *Neuroimage*. 2020;206:116338.
  101. Pirttimaki T, Salo RA, Shatillo A, Kettunen MI, Paasonen J, Sierra A, et al. Implantable RF-coil with multiple electrodes for long-term EEG-fMRI monitoring in rodents. *J Neurosci Methods*. 2016;274:154–63.
  102. Becq GJC, Habet T, Collomb N, Faucher M, Delon-Martin C, Coizet V, et al. Functional connectivity is preserved but reorganized across several anesthetic regimes. *Neuroimage*. 2020;219:116945.
  103. Schlegel F, Schroeter A, Rudin M. The hemodynamic response to somatosensory stimulation in mice depends on the anesthetic used: Implications on analysis of mouse fMRI data. *Neuroimage*. 2015;116:40–9.
  104. Silva AC, Koretsky AP, Duyn JH. Functional MRI impulse response for BOLD and CBV contrast in rat somatosensory cortex. *Magn Reson Med*. 2007;57:1110–8.
  105. Bennett CM, Wolford GL, Miller MB. The principled control of false positives in neuroimaging. *Soc Cogn Affect Neurosci*. 2009;4:417–22.
  106. He Y, Evans A. Graph theoretical modeling of brain connectivity. *Curr Opin Neurol*. 2010;23:341–50.
  107. Pearce PS, Wu Y, Rapuano A, Kelly KM, de Lanerolle N, Pan JW. Metabolic injury in a variable rat model of post-status epilepticus. *Epilepsia*. 2016;57:1978–86.
  108. Filibian M, Frasca A, Maggioni D, Micotti E, Vezzani A, Ravizza T. In vivo imaging of glia activation using 1H-magnetic resonance spectroscopy to detect putative biomarkers of tissue epileptogenicity. *Epilepsia*. 2012;53:1907–16.
  109. Alvestad S, Hammer J, Qu H, Haberg A, Ottersen OP, Sonnewald U. Reduced astrocytic contribution to the turnover of glutamate, glutamine, and GABA characterizes the latent phase in the kainate model of temporal lobe epilepsy. *J Cereb Blood Flow Metab*. 2011;31:1675–86.
  110. Pascente R, Frigerio F, Rizzi M, Porcu L, Boido M, Davids J, et al. Cognitive deficits and brain myo-Inositol are early biomarkers of epileptogenesis in a rat model of epilepsy. *Neurobiol Dis*. 2016;93:146–55.
  111. van der Hel WS, van Eijnsden P, Bos IW, de Graaf RA, Behar KL, van Nieuwenhuizen O, et al. In vivo MRS and histochemistry of status epilepticus-induced hippocampal pathology in a juvenile model of temporal lobe epilepsy. *NMR Biomed*. 2013;26:132–40.
  112. Guo J, Gang Z, Sun Y, Laine A, Small SA, Rothman DL. In vivo detection and automatic analysis of GABA in the mouse brain with MEGA-PRESS at 9.4 T. *NMR Biomed*. 2018;31:e3837.
  113. Nordengen K, Heuser C, Rinholm JE, Matalon R, Gundersen V. Localisation of N-acetylaspartate in oligodendrocytes/myelin. *Brain Struct Funct*. 2015;220:899–917.
  114. Petroff OA, Errante LD, Rothman DL, Kim JH, Spencer DD. Glutamate-glutamine cycling in the epileptic human hippocampus. *Epilepsia*. 2002;43:703–10.
  115. Ramadan S, Lin A, Stanwell P. Glutamate and glutamine: a review of in vivo MRS in the human brain. *NMR Biomed*. 2013;26:1630–46.
  116. Wellard RM, Briellmann RS, Prichard JW, Syngieniotis A, Jackson GD. Myoinositol abnormalities in temporal lobe epilepsy. *Epilepsia*. 2003;44:815–21.
  117. Bankstahl M, Bankstahl JP. Recent advances in radiotracer imaging hold potential for future refined evaluation of epilepsy in veterinary neurology. *Front Vet Sci*. 2017;4:218.
  118. Bankstahl JP, Bankstahl M. Imaging mechanisms of drug resistance in experimental models of epilepsy. In: Bernasconi A, Koepp M, Bernasconi N, editors. *Imaging Biomarkers in Epilepsy*. Cambridge: Cambridge University Press; 2019. p. 148–56.
  119. Reddy SD, Younus I, Sridhar V, Reddy DS. Neuroimaging biomarkers of experimental epileptogenesis and refractory Epilepsy. *Int J Mol Sci*. 2019;20:220.
  120. Dedeurwaerdere S, Shultz SR, Federico P, Engel J Jr. Workshop on Neurobiology of Epilepsy appraisal: new systemic imaging technologies to study the brain in experimental models of epilepsy. *Epilepsia*. 2014;55:819–28.
  121. Mannheim JG, Mamach M, Reder S, Traxl A, Mucha N, Disselhorst JA, et al. Reproducibility and comparability of preclinical PET imaging data: a multicenter small-animal PET study. *J Nucl Med*. 2019;60:1483–91.
  122. Dirnagl U, Fisher M. International, multicenter randomized preclinical trials in translational stroke research: it's time to act. *J Cereb Blood Flow Metab*. 2012;32:933–5.
  123. Goertzen AL, Bao Q, Bergeron M, Blankemeyer E, Blinder S, Canadas M, et al. NEMA NU 4-2008 comparison of preclinical PET imaging systems. *J Nucl Med*. 2012;53:1300–9.
  124. McDougald W, Vanhove C, Lehnert A, Lewellen B, Wright J, Mingarelli M, et al. Standardization of preclinical PET/CT imaging to improve quantitative accuracy, precision, and reproducibility: a multicenter study. *J Nucl Med*. 2020;61:461–8.
  125. Judenhofer MS, Wehrl HF, Newport DF, Catana C, Siegel SB, Becker M, et al. Simultaneous PET-MRI: a new approach for functional and morphological imaging. *Nat Med*. 2008;14:459–65.
  126. Okamura N, Harada R, Ishiki A, Kikuchi A, Nakamura T, Kudo Y. The development and validation of tau PET tracers: current status and future directions. *Clin Transl Imaging*. 2018;6:305–16.
  127. Abraham A, Luurtsema G, Bauer M, Karch R, Lubberink M, Pataria E, et al. Peripheral metabolism of (R)-[11C]vepamil in epilepsy patients. *Eur J Nucl Med Mol Imaging*. 2008;35:116–23.
  128. Nguyen DL, Wimberley C, Truillet C, Jegou B, Caille F, Pottier G, et al. Longitudinal positron emission tomography imaging

- of glial cell activation in a mouse model of mesial temporal lobe epilepsy: toward identification of optimal treatment windows. *Epilepsia*. 2018;59:1234–44.
129. Bascunana P, Thackeray JT, Bankstahl M, Bengel FM, Bankstahl JP. Anesthesia and preconditioning induced changes in mouse brain [(18)F] FDG uptake and kinetics. *Mol Imaging Biol*. 2019;21:1089–96.
  130. Deleye S, Verhaeghe J, Wyffels L, Dedeurwaerdere S, Stroobants S, Staelens S. Towards a reproducible protocol for repetitive and semi-quantitative rat brain imaging with (18) F-FDG: exemplified in a memantine pharmacological challenge. *Neuroimage*. 2014;96:276–87.
  131. Toyama H, Ichise M, Liow JS, Vines DC, Seneca NM, Modell KJ, et al. Evaluation of anesthesia effects on [18F]FDG uptake in mouse brain and heart using small animal PET. *Nucl Med Biol*. 2004;31:251–6.
  132. Hendrich KS, Kochanek PM, Melick JA, Schiding JK, Statler KD, Williams DS, et al. Cerebral perfusion during anesthesia with fentanyl, isoflurane, or pentobarbital in normal rats studied by arterial spin-labeled MRI. *Magn Reson Med*. 2001;46:202–6.
  133. Vines DC, Green DE, Kudo G, Keller H. Evaluation of mouse tail-vein injections both qualitatively and quantitatively on small-animal PET tail scans. *J Nucl Med Technol*. 2011;39:264–70.
  134. Eriksson O, Wallberg A, Syvanen S, Josephsson R, Langstrom B, Bergstrom M. A computerized infusion pump for control of tissue tracer concentration during positron emission tomography in vivo pharmacokinetic/pharmacodynamic measurements. *BMC Med Phys*. 2008;8:2.
  135. Funk T, Sun M, Hasegawa BH. Radiation dose estimate in small animal SPECT and PET. *Med Phys*. 2004;31:2680–6.
  136. Turner PV, Brabb T, Pekow C, Vasbinder MA. Administration of substances to laboratory animals: routes of administration and factors to consider. *J Am Assoc Lab Anim Sci*. 2011;50:600–13.
  137. Zanotti-Fregonara P, Chen K, Liow JS, Fujita M, Innis RB. Image-derived input function for brain PET studies: many challenges and few opportunities. *J Cereb Blood Flow Metab*. 2011;31:1986–98.
  138. Meganck JA, Liu B. Dosimetry in Micro-computed tomography: a review of the measurement methods, impacts, and characterization of the quantum GX imaging system. *Mol Imaging Biol*. 2017;19:499–511.
  139. Kersemans V, Thompson J, Cornelissen B, Woodcock M, Allen PD, Buls N, et al. Micro-CT for anatomic referencing in PET and SPECT: radiation dose, biologic damage, and image quality. *J Nucl Med*. 2011;52:1827–33.
  140. El Ali HH, Bodholdt RP, Jorgensen JT, Myschetzky R, Kjaer A. Importance of Attenuation Correction (AC) for small animal PET imaging. *Diagnostics (Basel)*. 2012;2:42–51.
  141. Bini J, Izquierdo-Garcia D, Mateo J, Machac J, Narula J, Fuster V, et al. Preclinical evaluation of MR attenuation correction versus CT attenuation correction on a sequential whole-body MR/PET scanner. *Invest Radiol*. 2013;48:313–22.
  142. Immonen R, Harris NG, Wright D, Johnston L, Manninen E, Smith G, et al. Imaging biomarkers of epileptogenicity after traumatic brain injury - Preclinical frontiers. *Neurobiol Dis*. 2019;123:75–85.
  143. Casillas-Espinosa PM, Andrade P, Santana-Gomez C, Paananen T, Smith G, Ali I, et al. Harmonization of the pipeline for seizure detection to phenotype post-traumatic epilepsy in a preclinical multicenter study on post-traumatic epileptogenesis. *Epilepsy Res*. 2019;156:106131.
  144. NEMA. Standards Publication NU 2–2007, Performance Measurements of Positron Emission Tomographs. Rosslyn: National Electrical Manufacturers Association; 2007.
  145. Mannheim JG, Kara F, Doorduyn J, Fuchs K, Reischl G, Liang S, et al. Standardization of Small Animal Imaging-Current Status and Future Prospects. *Mol Imaging Biol*. 2018;20:716–31.
  146. Schulz K, Sydekum E, Krueppel R, Engelbrecht CJ, Schlegel F, Schroter A, et al. Simultaneous BOLD fMRI and fiber-optic calcium recording in rat neocortex. *Nat Methods*. 2012;9:597–602.
  147. Cui M, Zhou Y, Wei B, Zhu XH, Zhu W, Sanders MA, et al. A proof-of-concept study for developing integrated two-photon microscopic and magnetic resonance imaging modality at ultrahigh field of 16.4 tesla. *Sci Rep*. 2017;7:2733.
  148. Duffy BA, Choy M, Chuapoco MR, Madsen M, Lee JH. MRI compatible optrodes for simultaneous LFP and optogenetic fMRI investigation of seizure-like afterdischarges. *Neuroimage*. 2015;123:173–84.
  149. Lee JH, Durand R, Gradinaru V, Zhang F, Goshen I, Kim DS, et al. Global and local fMRI signals driven by neurons defined optogenetically by type and wiring. *Nature*. 2010;465:788–92.
  150. Desai M, Kahn I, Knoblich U, Bernstein J, Atallah H, Yang A, et al. Mapping brain networks in awake mice using combined optical neural control and fMRI. *J Neurophysiol*. 2011;105:1393–405.
  151. Frangi AF, Niessen WJ, Vincken KL, Viergever MA. *Multiscale Vessel Enhancement Filtering*. Berlin, Heidelberg: Springer; 1998.
  152. Jerman T. Jerman Enhancement Filter. GitHub. Accessed September 18, 2020. <https://github.com/timjerman/JermanEnhancementFilter>
  153. Hayward NM, Immonen R, Tuunanen PI, Nde-Ekane XE, Grohn O, Pitkanen A. Association of chronic vascular changes with functional outcome after traumatic brain injury in rats. *J Neurotrauma*. 2010;27:2203–19.
  154. Brackhan M, Bascunana P, Postema JM, Ross TL, Bengel FM, Bankstahl M, et al. Serial quantitative TSPO-targeted PET reveals peak microglial activation up to 2 weeks after an epileptogenic brain insult. *Journal of Nuclear Medicine*. 2016;57(8):1302–8.

## SUPPORTING INFORMATION

Additional supporting information can be found online in the Supporting Information section at the end of this article.

**How to cite this article:** van Vliet EA, Immonen R, Prager O, Friedman A, Bankstahl JP, Wright DK, et al. A companion to the preclinical common data elements and case report forms for in vivo rodent neuroimaging: A report of the TASK3-WG3 Neuroimaging Working Group of the ILAE/AES Joint Translational Task Force. *Epilepsia Open*. 2025;10(Suppl. 1):S136–S182. <https://doi.org/10.1002/epi4.12643>